Front. Earth Sci. 2021, 15(3): 649–675
https://doi.org/10.1007/s11707-021-0881-1

RESEARCH ARTICLE

3D structural modeling integrated with seismic attribute and petrophysical evaluation for hydrocarbon prospecting at the Dhulian Oilfield, Pakistan

Umair KHAN[1], Baoyi ZHANG (✉)[1], Jiangfeng DU[2], Zhengwen JIANG[1]

1 MOE Key Laboratory of Metallogenic Prediction of Nonferrous Metals & Geological Environment Monitoring/ School of Geosciences & Info-Physics, Central South University, Changsha 410083, China
2 CNOOC Research Institute Co. Ltd., Beijing 10028, China

Abstract Surface and deep subsurface geological structural trends, stratigraphic features, and reservoir characteristics play important roles in assessment of hydrocarbon potential. Here, an approach that integrates digital elevation modelling, seismic interpretation, seismic attributes, three-dimensional (3D) geological structural modeling predicated on seismic data interpretation, and petrophysical analysis is presented to visualize and analyze reservoir structural trends and determine residual hydrocarbon potential. The digital elevation model is utilized to provide verifiable predictions of the Dhulian surface structure. Seismic interpretation of synthetic seismograms use two-way time and depth contour models to perform a representative 3D reservoir geological structure evaluation. Based on Petrel structural modeling efficiency, reservoir development indexes, such as the true 3D structural trends, slope, geometry type, depth, and possibility of hydrocarbon prospects, were calculated for the Eocene limestone Chorgali, upper Paleocene limestone Lockhart, early Permian arkosic sandstone Warcha, and Precambrian Salt Range formations. Trace envelope, instantaneous frequency, and average energy attribute analyses were utilized to resolve the spatial predictions of the subsurface structure, formation extrusion, and reflector continuity. We evaluated the average porosity, permeability, net to gross ratio, water saturation, and hydrocarbon saturation of early Eocene limestone and upper Paleocene limestone based on the qualitative interpretation of well log data. In summary, this integrated study validates 3D stratigraphic structural trends and fault networks, facilitates the residual hydrocarbon potential estimates, and reveals that the Dhulian area has a NE to SW (fold axis) thrust-bounded salt cored anticline structure, which substantiates the presence of tectonic compression. The thrust faults have fold axes trending from ENE to WSW, and the petrophysical analysis shows that the mapped reservoir is of good quality and has essential hydrocarbon potential, which can be exploited economically.

Keywords surface model, seismic interpretation, subsurface structural model, attributes, hydrocarbon potential

1 Introduction

Hydrocarbon exploration is increasingly performed under more complex geological conditions; therefore, systematic operations are needed to optimize oil production to meet global energy needs (Nanda, 2016). Three-dimensional geological modeling is needed to express geological characteristics (e.g., shapes of geological structures, relationships among geological bodies, spatial distributions of geophysical and geochemical properties of geological bodies) in an appropriate computer data structure (Houlding, 1994; Lajaunie et al., 1997; Mallet, 2002; Wu et al., 2005; Zhang et al., 2018). Therefore, the use of integrated methods, e.g., digital elevation models (DEMs), surface slope analysis, 2D seismic interpretation, and 3D structural modeling based on seismic interpretation, seismic attributes, and petrophysical analysis of reservoirs, can identify geometric features, reveal internal and external reservoir structures, and quantitatively evaluate reservoir properties (e.g., lithology, porosity, permeability, net pay zone thickness, water saturation, and hydrocarbon saturation). The results obtained from such work can be applied to increase productivity, revitalize oil fields, predict future reservoir productivity, and indicate accurate financial consequences for oil and

Received October 26, 2020; accepted February 7, 2021

E-mail: zhangbaoyi@csu.edu.cn

gas companies (Dowd, 1994; Asquith and Krygowski, 2004; Shah and Abdullah, 2017; Ehsan et al., 2019; Wang et al., 2019). A high-quality forecast of hydrocarbon resources can be achieved by integrating seismic, well log, and other geological data that are commonly used in hydrocarbon exploration and development studies (Shah and Abdullah, 2017). Remote sensing (RS) and geographical information systems (GISs) are primarily used for the delineation of surface features for petroleum research (Hart and Balch, 2000), although 3D geometric modeling is becoming more important for exploring reservoir structures, which is a key step in hydrocarbon prospecting. Three-dimensional geological structural modeling based on seismic interpretation is to identify reservoir geometry in terms of hydrocarbon prospects. The key elements of the structural model are the interpreted horizons and fault surfaces. In addition, the use of seismic attribute analysis (such as trace envelope, instantaneous frequency, and average energy attribute analyses) can improve seismic interpretation analysis (Dowd, 1994; Hesthammer and Fossen, 1997; Everett et al., 2002; Asquith and Krygowski, 2004; Ishak et al., 2018; Ngui et al., 2018). The importance of data integration is generally based on its ability to increase the efficiency of displaying complex geological structural problems (Ishak et al., 2018).

The study area is located in the active foreland folds and thrust belts of the Himalayan orogenesis on the Potwar Plateau. Researchers have integrated several geological methods as well as geophysical methods, primarily seismic reflection schemes for petroleum evaluation, and they provide important information for accurately revealing subsurface geological structures and establishing consistent and accurate correlations (Butler et al., 1987; Adeoye and Enikanselu, 2009). A number of wells have become unproductive as a consequence of complex subsurface structures. In the 1950s, several predictions were inadequately verified, but with more seismic evidence, they were re-examined in the 1960s. Based on comprehensive wire-line and seismic data, various evaluations were conducted in the 1980s and 1990s to illustrate the overall structure and deformation mechanics from the perspective of hydrocarbon evaluation. In the northern Potwar deformed zone (NPDZ), Jaswal et al. (1997) and Jadoon et al. (2015) demonstrated a multifaceted distortion utilizing seismic, borehole, and paleomagnetic interpretations of the form of imbricates and duplex structures (Baker et al., 1988; Gee and Gee, 1989; Khan et al., 2018; Riaz et al., 2019). Previous studies on the Potwar basin have shown that the basin has major geological features and an essential history in petroleum exploration and production (Kadri, 1995; Fazeelat et al., 2010). The influential factors affecting hydrocarbon saturation include the trend of surface to deep subsurface geological structure and static reservoir properties. To quantify the hydrocarbon prospects of reservoirs, it is necessary to understand the characteristics and extent of the reservoir and its surrounding 3D geological structure behavior.

Therefore, this study aims to investigate surface geological structure trends, perform three-dimensional subsurface reservoir structural modeling, and characterize static reservoir properties using a combined set of seismic reflections, geophysical well logs, and DEM data. Simulation software was used to complete individual analysis goals, e.g., surface contouring, horizons and fault reconstructions on seismic reflection profiles, two-way time (TWT) and depth contour model construction, and perform representative three-dimensional evaluations of reservoir structure complexity. Based on the Petrel structural modeling functions (fault modeling, pillar gridding, and vertical layering), reservoir development indexes at the Dhulian Oilfield, Pakistan, such as true 3D reservoir structural trends, slope, geometry type, depth and hydrocarbon prospect potential, were calculated. The petrophysical parameters, including lithology, porosity, permeability, water saturation, and net to gross ratio, were determined to map hydrocarbon-bearing reservoirs. The integrated 3D reservoir structure and petrophysical results were then used to identify the hydrocarbon prospects. The main advantage of this integrated study is that it provides complete surface to deep subsurface information to improve the reliability of 3D geological interpretation in hydrocarbon prospecting compared with that of a single method. This research will increase the prospects of hydrocarbon production and exploration in the Dhulian oilfield, Potwar basin, Pakistan.

2 Geology and tectonic setting

The study area is located between latitude 33°12'41"N and longitude 72°12'00"E in the central part of the Potwar subbasin (Fig. 1(a)). The area experienced a compression mode and complex traction destruction (Ishak et al., 2018). Knowledge of the stratigraphic subdivision in the Potwar subbasin has been gained from exploratory wells drilled by the Oil and Gas Development Company Limited (OGDCL) (Fig. 2). Structurally, the Dhulian surface is an almost symmetrical anticline with a maximum inclination of 30° to 35°, and the fold axis tends towards ENE-WSW and descends approximately 4° to 5° at both ends, extending along with the steps to the nearby Khaur fold (Jaswal et al., 1997; Fajana et al., 2019). The Dhulian fold is flanked by the Soan syncline to the south and the tight Pindi Gheb to the north. This area is fertile area of oil and gas occurrence. The first commercial discovery of the Himalayan foreland area occurred in the Potwar subbasin of Khaur in 1994. This subbasin has multiple structural indications (Khan et al., 1986; Kemal, 1991; Wandrey et al., 2004; Moghal et al., 2007).

The Potwar subbasin experienced severe deformation during the Pliocene-Middle Pleistocene Himalayan orogenic process. The regional unconformity in the strata

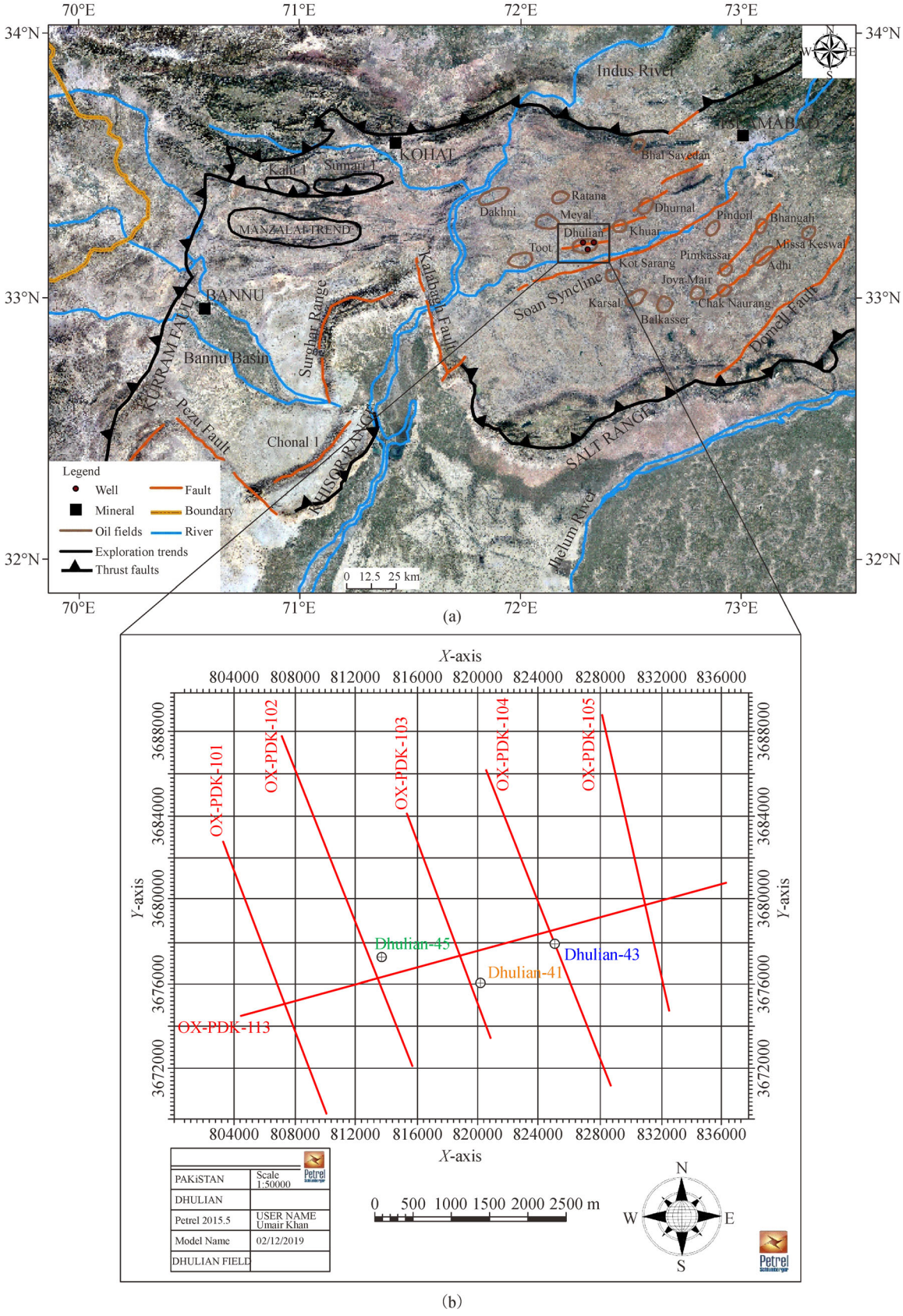

Fig. 1 (a) Geological map showing the major geological structural setting, and generalized oil and gas fields of the Potwar Basin in northern Pakistan. (b) Base map showing the location and orientation of the 2D reflection seismic lines (dip/strike).

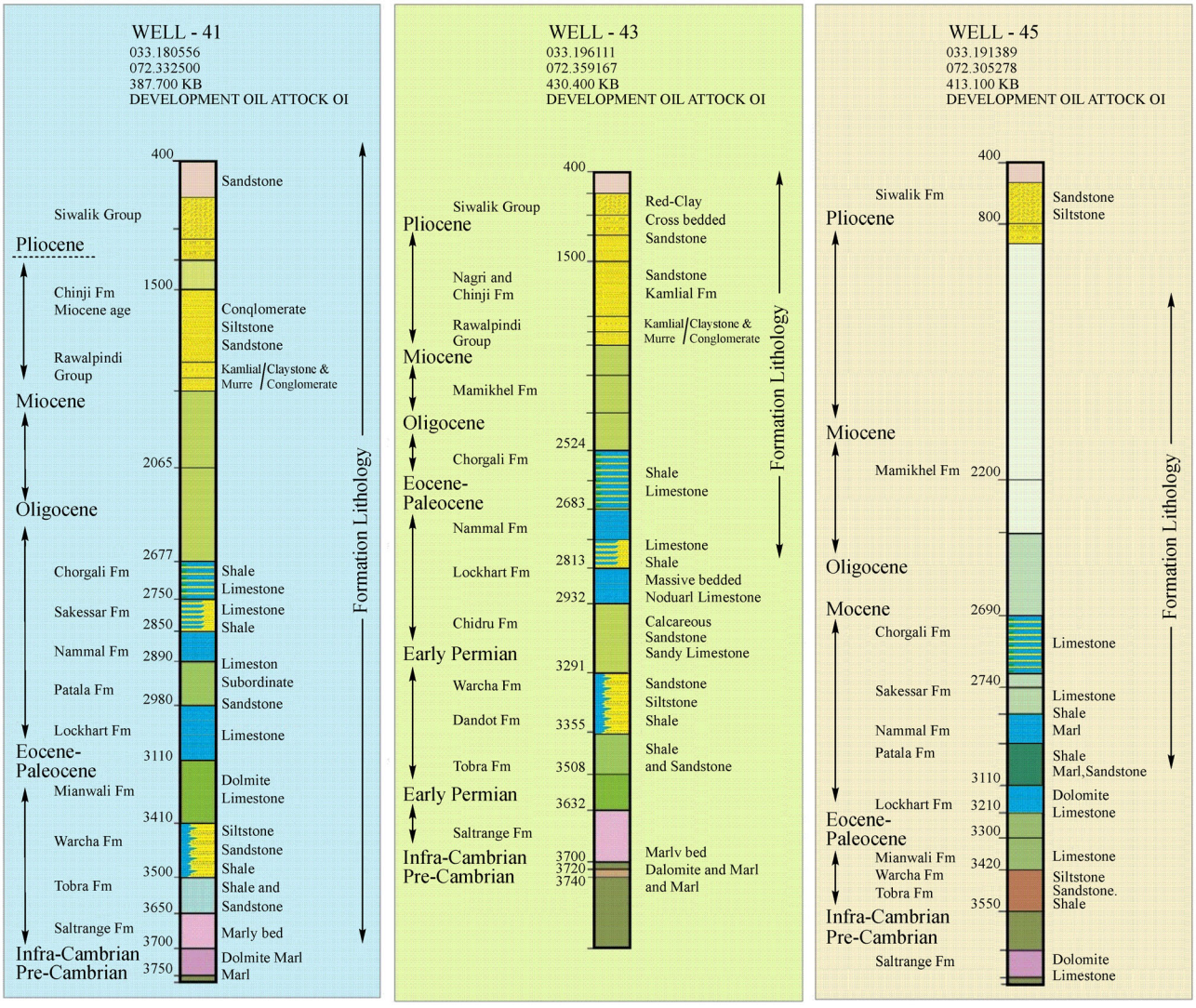

Fig. 2 Stratigraphic subdivision of (a) well 41, (b) well 43, and (c) well 45 in the Dhulain area of the Potwar Basin.

section of the basin reflects the authenticity of tectonic pulses. It is suggested that the Potwar Basin was formed in the western foothills of the Himalayas in northern Pakistan, which facilitated and controlled the formation of the present Dhulian Oilfield. It is bounded by the main boundary thrust (MBT) in the north and the Salt Range in the south (Gee and Gee, 1989). The basin is filled with thick Precambrian evaporates overlain by relatively thin platform deposits of Cambrian to Eocene age, followed by thick Miocene Pliocene molasses (Muni et al., 1990; Jaswal et al., 1997). The central, western, and eastern parts of the Potwar Plateau have completely different structural behaviors. A subsurface view of the Potwar subbasin indicates that the structure is regionally limited by boundary shocks of the leading edge. These thrusts tend to the NE from the SW in the eastern part, almost E to W in the central part, and from NW to SE in the western parts of the Potwar subbasin. Based on seismic interpretation, the structures of the Potwar region can be categorized into pop-up anticlines, snake-head anticlines, salt cored anticlines, and triangle zones. The main structure of the basin is the Soan syncline, which extends along the NE-SW direction. The faults of the entire Dhulian oilfield typically present ENE-SSW trends and correspond to the Neogene deformation belt. The EW Soan syncline detaches this region into a less deformed southern Potwar platform zone (SPPZ) and a more deformed northern Potwar deformed zone (NPDZ) (Kazmi and Rana, 1982; Grelaud et al., 2002; Aamir and Siddiqui, 2006). The extremely dismembered NPDZ deformation framework immediately changes from east to west. It exhibits the presence of extensive synclines, compressed folds and closely spaced imbricate thrusts. The eastern NPDZ impersonates the buried thrust front along with the foreland syncline,

triangle zone, and hinterland-dipping imbricate stack farther northwards. However, the western NPDZ describes a prominent faulted anticline distanced through synclines along with a developing thrust. Jaswal et al. (1997) concluded that a ~55 km horizontal shortening occurred between the Soan syncline and main boundary thrust and projected a minimum rate of shortening of 18 mm/yr. Deep Infra-Cambrian evaporate sediments characterize the Potwar subsurface geology.

3 Datasets and methods

The components of this study can be divided into six parts, e.g., terrain surface modeling, seismic interpretation, 3D reservoir structural modeling, seismic attribute analysis, petrophysical analysis, and hydrocarbon volumetric estimation. Our study used a digital elevation model (DEM), suite of wire-line logs (e.g., gamma-ray, bulk density, neutron porosity, spontaneous potential, resistivity and sonic) of well 41 (33°10'50″N; 72° 19' 56"E), well 43 (33° 11'45"N; 72°21'33"E), well 45 (33°11'29"N; 72°18'19"E) and 35-fold two-dimensional post-stack migrated seismic data in the field (Fig. 1(b)). Seismic and well log datasets were collected from the Directorate General of Petroleum Concessions (DGPC), which are available in the public domain and can be utilized for scientific and research purposes. Available seismic and well log data were loaded into Petrel™ 2015 Schlumberger and Geo-Graphix Suite-LMKR software. The data were checked for quality (QC) and harmonized in clearly defined databases. The stepwise integrated methodology proposed here is shown in Fig. 3.

3.1 Digital elevation modeling

The digital elevation model (DEM) is one of the fundamental spatial datasets in geographic information systems (GIS) (Jaboyedoff et al., 2009). Sharp fluctuations in elevation are a sign of changes in the geological structure. Commonly, modeling the surface structure can partly reveal the depth structure of the exploration target. Therefore, the surface model can be classified to evaluate surface topographic trends from a three-dimensional perspective (Blythe et al., 2000; Chen et al., 2015). The surface geological structure of the Dhulian area of the Potwar basin is fairly complex. A contour-based digital elevation model has been constructed. The terrain data were accumulated in XYZ coordinates from Google Earth, DEM generation, DEM manipulation, and DEM interpretation, and DEM visualization processes were performed in Surfer15 and ArcGIS software. A DEM based on contours consists of a set of contour lines that are "labeled" with the corresponding elevation values. We use an interval of 100 meters between the contours. Contour lines are stored in ordered coordinates and can be considered polylines or polyline arcs containing elevation values (Silva et al., 2007; Burrough et al., 2015).

3.2 Seismic data interpretation

A seismic survey was designed based on the prevailing structural elements. Therefore, a number of seismic reflection profiles were utilized to investigate different fault dips and reservoir structural trends. Seismic interpretations were performed in several stages, and a base map located in the 42-N Trans-Mercator Macrocosm (UTM) zone was created by loading navigation and SEG-Y records in the Petrel™ 2015 Schlumberger modeling software (Fig. 1(b)). The primary process of seismic interpretation is to correlate seismic data with well log data to obtain consistent stratigraphic sequences and establish the relationship between seismic reflections and stratigraphy. Therefore, the logging data have been used to verify and to standardize the designations of stratigraphic units. The available well top data of Dhulian-43 well were overlaid on the OX-PDK-104 dip survey line, and OX-PDK-113 strike survey line, for formation location analysis and judgment, which can better explain and define the formation attributes (Fig. 4). The seismic stratigraphic classification is inconsistent with the combined well top data. High coherence of reflectors allows smooth auto-tracking of horizons except where the horizons of interest were tracked along specific weak amplitude peaks or troughs in the seismic profile. Sonic and density logs were utilized to generate synthetic seismograms to define the correct horizons. Regional geological structures as six prominent stratigraphic units were selected and completely delineated: the Eocene limestone Chorgali Formation, upper Paleocene limestone Lockhart Formation, early Permian arkosic sandstone Warcha Formation, and Precambrian saline series Salt Range Formation. The horizons were marked on each seismic dip/strike cross-section by differentiating marker strata and other corresponding points assigned to well logs with primary reflections on the seismic cross-section (Fig. 4). Consequential faults were selected that include essential elements for characterizing the structural pattern and entrapment style of the hydrocarbons. Two-dimensional time structural models, where the values are in two-way seismic travel time, were equipped for each interpreted stratigraphic unit. Additionally, depth contour models were established, and their contours were calculated by multiplying the estimated average velocity function for the designated horizon by the corresponding time grid. Typically, structural depth contour models contribute to the configuration of the horizon, which is similar to two-way time contour models (Ishak et al., 2018). Two-way time-to-depth transfiguration was executed by using the following formula:

$$S = (V \times T)/2, \quad (1)$$

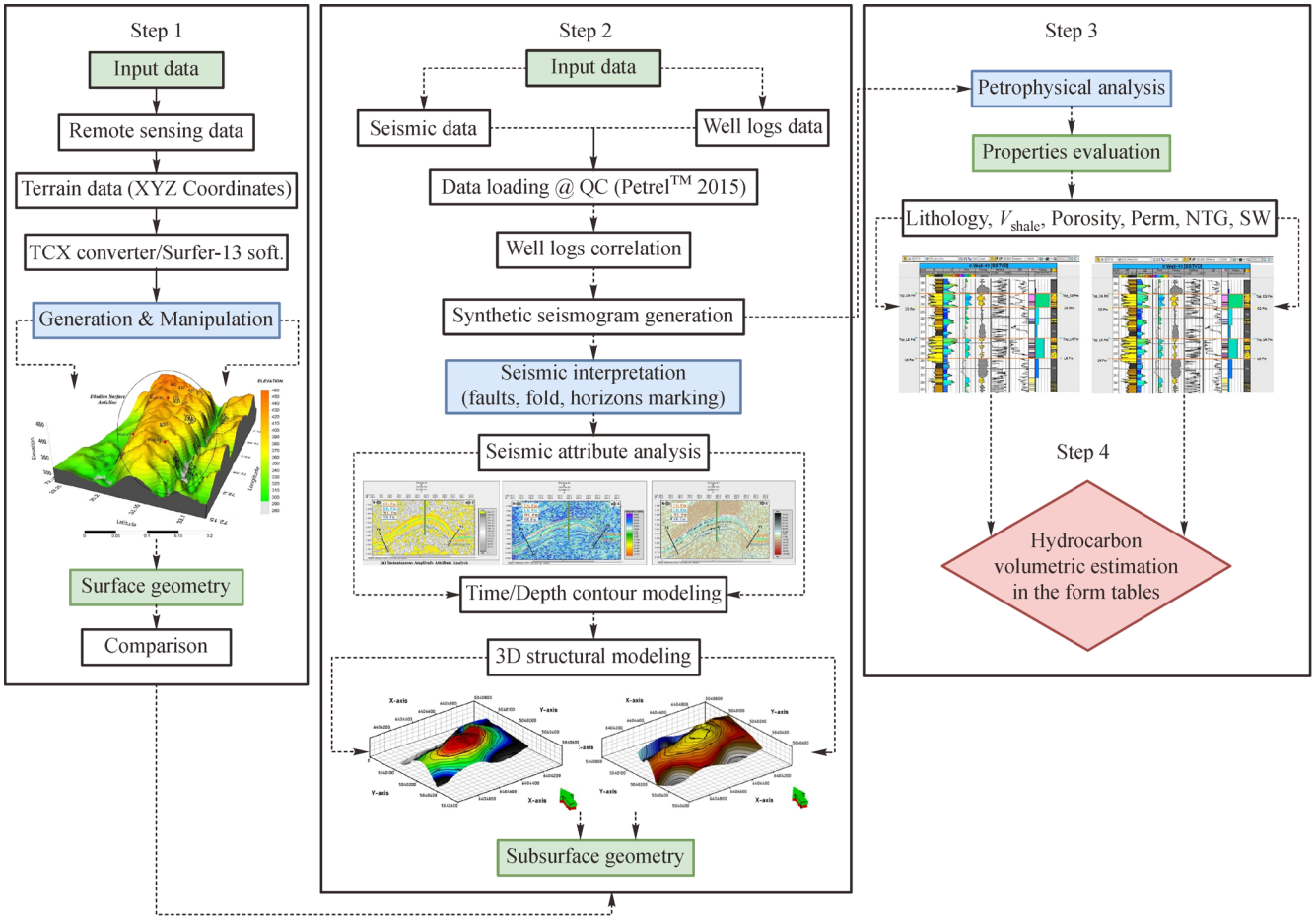

Fig. 3 Step-by-step workflow of integrated methods for surface and underground 3D geological structural modeling and petrophysical property evaluation.

where S is the depth of the horizon, V is the average velocity, and T is the two-way time of the horizon scrutinized from the seismic profile.

3.3 3D Geological structural modeling

Over the last 25 years, the approach of three-dimensional geological structural modeling has led to enormous developments in our understanding of overall reservoir geometry. Three-dimensional structural geological modeling follows the interpretation of a prior knowledge of subsurface geological structure (Hart and Balch, 2000; Bitrus et al., 2016). Petrel is a PC-based workflow application for subsurface interpretation and modeling, and it can create a large scale 3D reservoir structural model relatively quickly with a specific modeling workflow. Generally, Petrel structural modeling is based on seismic data interpretation, which follows the process of fault modeling, pillar meshing, and vertical layering (Fagin, 1991). To develop a 3D structural geological model for each stratigraphic unit, Petrel's structural modeling framework was used to understand the realistic structural geometry of the reservoir in this study. The imported files for each data object include six seismic reflection profiles, wellhead, well top, and logging data. Structural TWT contours are the fundamental tool for deciphering three-dimensional sinuses because they provide distinct descriptions of the full three-dimensional shape of stratigraphic units (Stewart, 1999; Mehmood et al., 2016). First, surface polygons, faults networks and horizons corresponding to seismic faults are established (Fig. 5). In our experience, structural modeling rarely works smoothly by running the first step and proceeding to grid generation. Second, three-dimensional grids of horizontal and vertical line networks were used to describe the 3D geological model. The pillar gridding represents the basis of all modeling. The third step involves inserting the explained stratigraphic horizons into the pillar grid and observing grid increments and faults. The last step was to construct and outline the reservoir structure using a two-way time relationship to define the vertical stratification and orientation of the 3D stratigraphic units. Based on Petrel structural modeling efficiency, reservoir development indexes, such as true three-dimensional reservoir

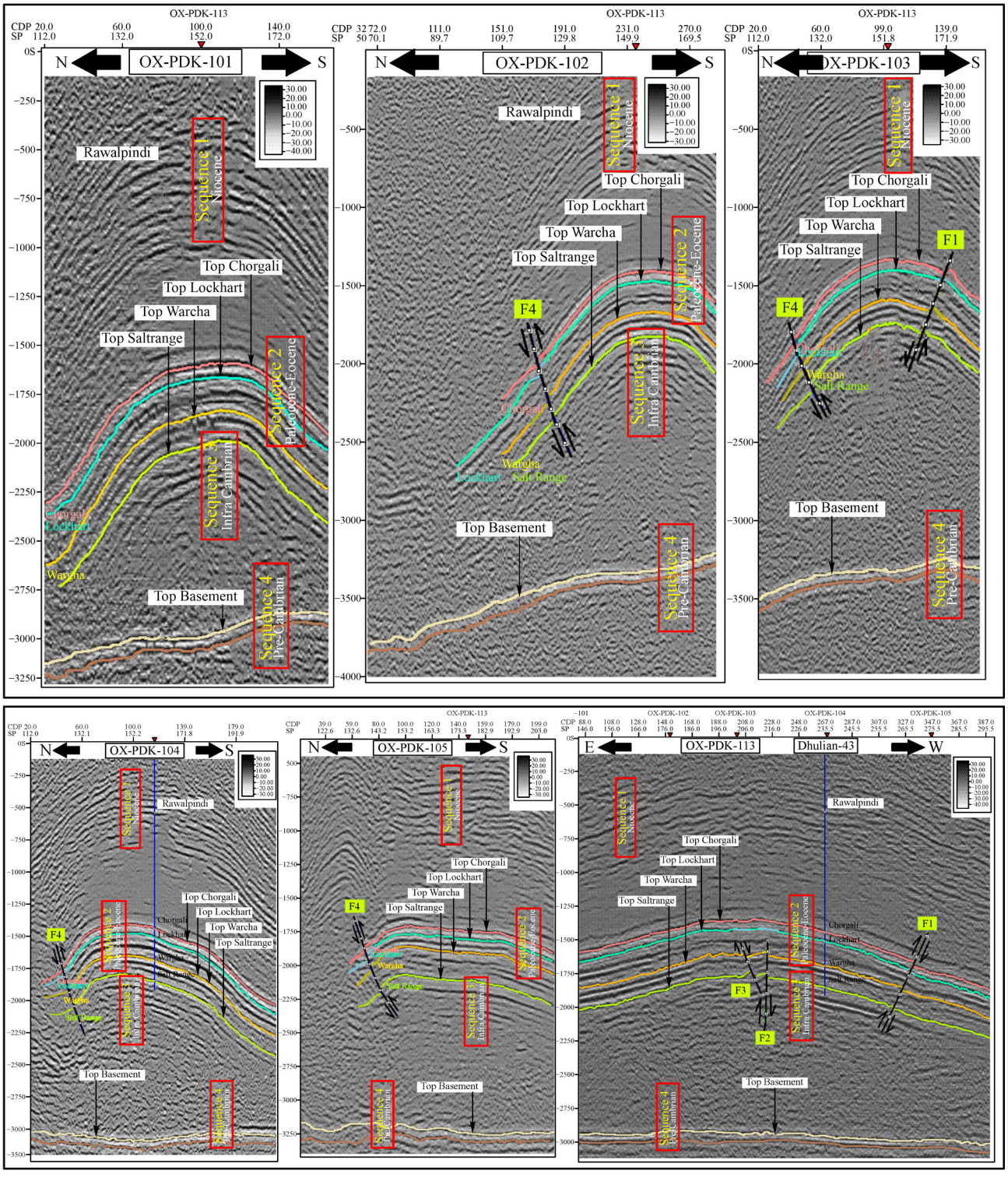

Fig. 4 Interpretation and reflection feature analysis of seismic cross-sections (OX-PDK-101, OX-PDK-102, OX-PDK-103, OX-PDK-104, OX-PDK-105, and OX-PDK-113) showing anticline structures and major faults. The interpreted stratigraphic units can be exported and processed to create 2D time/depth contour models.

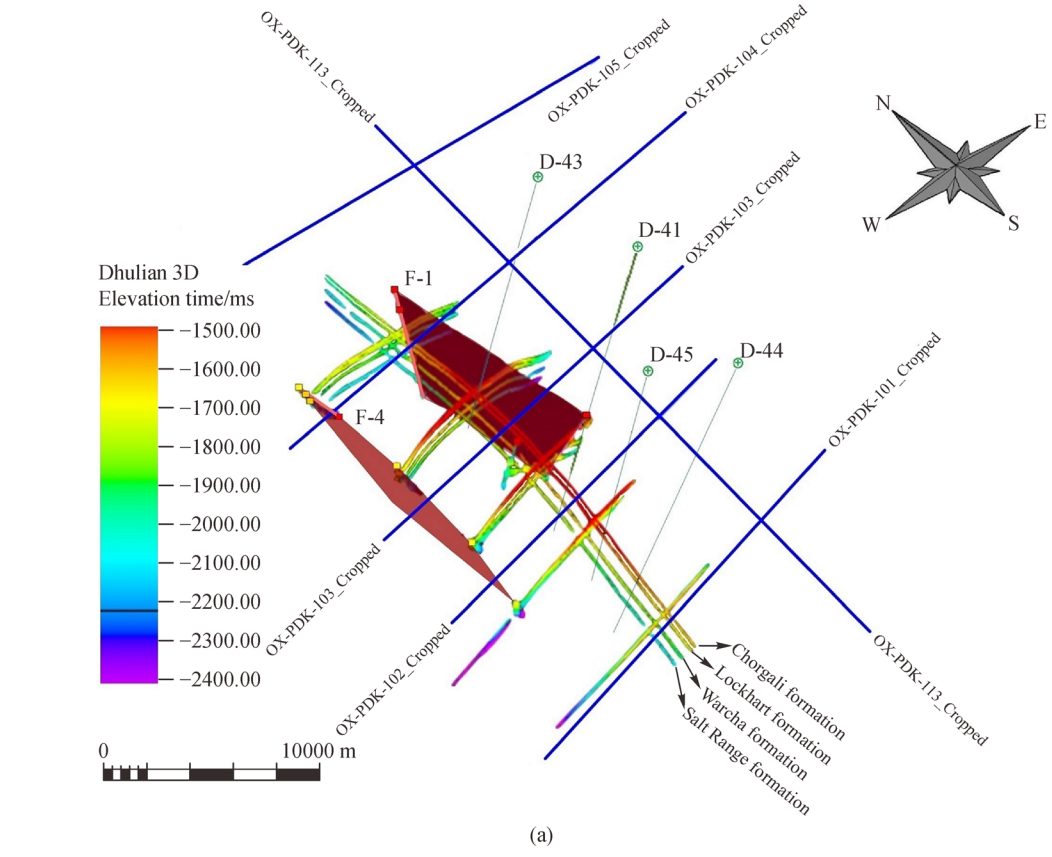

(a)

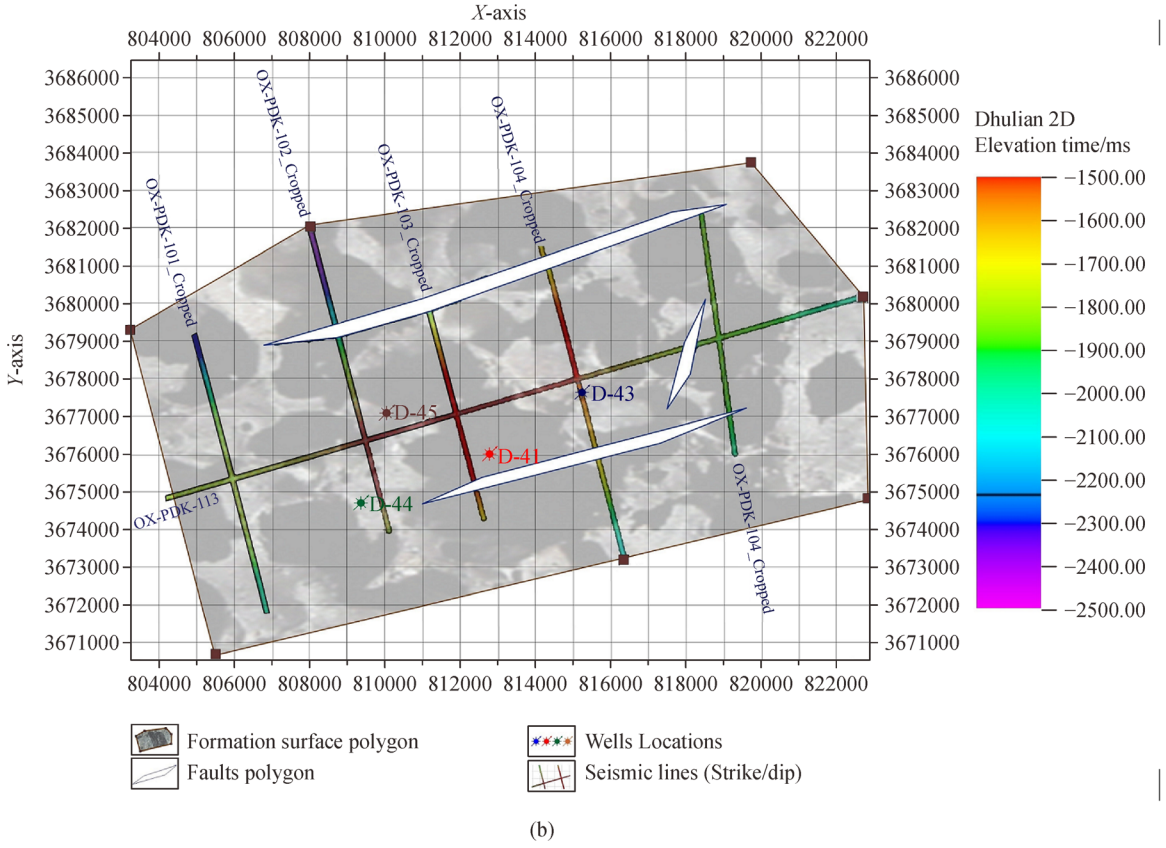

(b)

Fig. 5 (a) Three-dimensional view of the interpreted horizons, fault separation and wells. (b) Formation surface polygons along with fault polygons.

structural trends, slope, channel characteristics, geometry type, depth and possibility of hydrocarbon prospect potential, were calculated. Finally, through the application of Petrel structural modeling, we constructed 3D structural models for the Eocene limestone Chorgali Formation, upper Paleocene limestone Lockhart Formation, early Permian arkosic sandstone Warcha Formation, and Precambrian saline series Salt Range Formation.

3.4 Seismic attribute analysis

After a comprehensive interpretation of seismic data, a seismic attribute analysis can be utilized to further improve the interpretation of local details in complex structural areas or fault regions. The trace envelope attribute increases the reflector's strength, amplitude, and energy while increasing the essential characteristics of a seismic reflector (Wang et al., 2016). The trace envelope can be calibrated from a complicated trace, which is first proposed by Taner (2001), and it can be defined as follows:

$$CT(t) = [T(t) \ + tH(t)], \tag{2}$$

where $CT(t)$ stands for the complex trace; $T(t)$ represents the seismic trace; $H(t)$ represents Hilbert's transform of $T(t)$ and $H(t)$ is a 90° phase shift of $T(t)$. The trace envelope is calculated from the complex trace through the following formula:

$$E(t) \ = SQRT[T2(t) \ + H2(t)]. \tag{3}$$

On dip seismic line 104, the trace envelope attribute was used to distinguish the top and bottom stratigraphic units. In this study, other attributes (such as instantaneous frequency and average energy) can be effectively used to analyze each symbol to improve the spatial prediction of the subsurface geological structure, reservoir extrusion, reflector continuity, and layer thickness and to help us predict the physical properties of the formation in potential areas.

3.5 Petrophysical analysis

Interpretation of well log data was performed by correlating each response curve to delineate hydrocarbon-bearing reservoirs via appropriate petrophysical parameters, such as lithology sections, shale volume, porosity, effective porosity, permeability, water saturation, net to gross ratio, and hydrocarbon saturation of the reservoirs in the Dhulian oilfield. Gamma-ray and resistivity logs were employed to determine the lithology and reservoir spacing. The use of gamma-ray deflection with incremental resistivity is performed to determine reservoir spacing while considering the rightward deflection of gamma rays relevant to resistivity decline, which indicates non-reservoir (shale) lithology (Szabó, 2011). The presence of shale in the reservoir, if not defined, usually affects the calculation of other properties of the reservoir, such as the porosity, permeability, water saturation, and hydrocarbon saturation (Ehsan and Gu, 2020). Initially, the gamma-ray index I_{GR} was adopted using Eq. 4 to recognize the volume of the shale by gamma-ray log values (Khan et al., 2013):

$$I_{GR} = [(GR_{log} - GR_{min})/(GR_{max} - GR_{min})], \tag{4}$$

where I_{GR} stands for the gamma ray index; GR_{log} represents the reading of the gamma-ray log; and GR_{min} is the lower limit of gamma rays in clean (carbonate) shale and the upper limit of gamma ray in shale. Furthermore, the volume of shale was obtained using the following formula:

$$V_{sh} = 1.7 - \left[\left(3.38 - (I_{GR} + 0.7)^2\right)\right]^{\frac{1}{2}}. \tag{5}$$

The density porosity equation was used to calculate the total porosity of the CG and LK reservoirs after estimating the volume of the shale:

$$\phi_D = [(\rho_{mat} \ - \rho_b)/(\rho_m - \rho_f)], \tag{6}$$

where ϕ_D represents the total porosity, ρ_{mat} represents the density of the matrix, ρ_f represents density of the fluid, and ρ_b is the density of the bulk.

The effective porosity (Aguilera and Aguilera, 2004; Shah and Abdullah, 2016) was calculated using the following formula:

$$\phi_E = [(\phi_T) \times (1 - V_{sh})], \tag{7}$$

where ϕ_E describes the effective porosity, ϕ_T represents the total porosity, and V_{sh} is the shale content in volume units.

Water saturation was determined by Simandoux method (Archie, 1942), where S_w stands for water saturation, R_w represents formation water resistivity, V_{sh} is the shale volume, ϕ is the porosity, R_t is the true resistivity, and R_{sh} is the shale resistivity:

$$S_w = \left(\frac{0.4 \times R_w}{\phi^2}\right)\left[\frac{V_{sh}}{R_{sh}}\sqrt{\left(\frac{V_{sh}}{R_{sh}}\right)^2 + \frac{5\phi^2}{R_t \times R_w}}\right]. \tag{8}$$

Permeability was calculated from an estimate of effective porosity and nonreducible water saturation (Ameloko and Owoseni, 2015) using Eq. (9):

$$K = [307 + (2655)\phi^2] - 34540(\varnothing S_{wirr}^2), \tag{9}$$

where K stands for permeability, and S_{wirr} represents nonrestorable water saturation estimation.

The net to gross (NTG) ratio was calculated using Eq. (10):

$$NTG = [1 - V_{shale} \ ]. \tag{10}$$

3.6 Hydrocarbon volume estimation

The average values of the petrophysical parameters for the interpreted reservoirs were calculated to achieve the corresponding value for calculating in situ hydrocarbons. This calculation is essential because it concludes whether the company proceeds to further exploration and production activities in the field (Gee and Gee, 1989; Awais et al., 2019). The estimation of in situ hydrocarbons was conducted utilizing the following standard volumetric estimation expression:

$$STOIIP = \left(\frac{7758 \times Ah\phi \times (1 - S_{\mathrm{w}})}{B_{\mathrm{oi}}}\right), \qquad (11)$$

where *STOIIP* represents the stock tank oil in place; A represents the area in acre; h is the reservoir thickness in feet; S_{w} is the water saturation in percentage; ϕ is the rock porosity in percentage; and B_{oi} is the oil formation volume factor.

4 Results and discussion

4.1 Digital elevation model

A quantitative DEM model was created for the Dhulian surface in digital form. It is essential first to examine digital elevation models to study the geological structure and understand the relationship between geological and topographic differences (Blythe et al., 2000; Burrough et al., 2015). The results obtained demonstrate the capability of utilizing geological contours modeled over DEMs for structural geological interpretation. The difference in elevation between the adjacent contour lines, called the contour interval, best showed the general shape of the terrain. Each contour line represents different elevation values, while slope and gentle elevation can be optically discerned in both two-dimensional and three-dimensional models. Proximate contours designate steep slopes, while wider equidistant distributions or inadequate contours indicate that the slope is relatively horizontal. To provide different ascensions, we utilize color gradients. The two-dimensional DEM model shows a terrain structure in the form of values, i.e., 470 m represents a high terrain area, while 270 m indicates a low terrain area (Fig. 6(a)). The three-dimensional DEM model additionally shows a distinct scenario (Fig. 6(b)). The region is postulated to be in compression mode and has a complex surface structure. The surface structure is a virtually symmetrical anticline with a maximum dip of 30° to 35°, which can be compared with the subsurface 3D reservoir model. Modeling surface structure can partially uncover the depth structure of the exploration target. The surface anticline is circumscribed by latitude 33°12'41"N and longitude 72°12'00"E in the eastern part of the Potwar subbasin.

4.2 Seismic data interpretation

Initially, seismic cross-sections were interpreted by integrating well data with seismic reflection data to understand the subsurface geology and structural characteristics. Seismic cross-sections show the displacement of the stratigraphic units in the Dhulian area, upper Indus Basin Pakistan. Based on the synthetic seismogram, we interpreted and predicted four stratigraphic surfaces, i.e., the Eocene limestone Chorgali Formation, upper Paleocene limestone Lockhart Formation, early Permian arkosic sandstone Warcha Formation, and Precambrian saline series Salt Range Formation, were interpreted. Fig. 4 shows the enacted seismic dip, and strike lines are oriented north to south. Pink, green, yellow, and light yellow colors denote the interpreted stratigraphic units. These prominent horizons constitute the target horizons for hydrocarbon exploration in the study area.

In the study area, according to the seismic reflection characteristics, four sets of seismic stratigraphic sequences were encountered. The stratigraphic constituent of the region appeared on six seismic sections and three wells (Figs. 2 and 4). In our study, four major sequences were observed by analyzing of the reflection terminations and observation of seismic reflectors in terms of their amplitude, continuity, configuration, frequency, and corresponding external geometries. According to the seismic reflection, various boundaries and continuities from top to bottom (youngest to oldest) are as follows: sequence 1 is the topmost sequence with parallel and weak to continuous reflection, representing the molasses structure of the Miocene era; sequence 2 has parallel and continuous reflections with high amplitude and high frequency, representing the conventional Potwar reservoirs in the Paleocene-Eocene period; sequence 3 has strong and moderate continuous reflections, with significant variations in thickness, representing the Cambrian-aged Salt range stratum which consist of salt and evaporite; and sequence 4 has continuous dark reflections at the bottom of the seismic profile, representing the Precambrian basement (Fig. 4). Based on the heterogeneity of geological reflections, two significant reverse faults, i.e., F1 and F4 have been identified. These back faults are the boundaries of the backline, and structural closures appear as anticline structures that are gently inclined (10°–20°) to the edges of faults F1 and F4. Structural and analytical interpretations reveal that the Dhulian area has a complex salt cored anticlinal structure, which confirms the existence of compression tectonics and the possibility of hydrocarbons.

The identification of the subsurface structure and its influence on the geometric relationship between the stratigraphic units is primarily predicated on the time and depth contour models because contour lines depict lines connecting the same elevation, which is why they are essential tools for analyzing seismic data (Adeoye and Enikanselu, 2009). Such models are conventionally

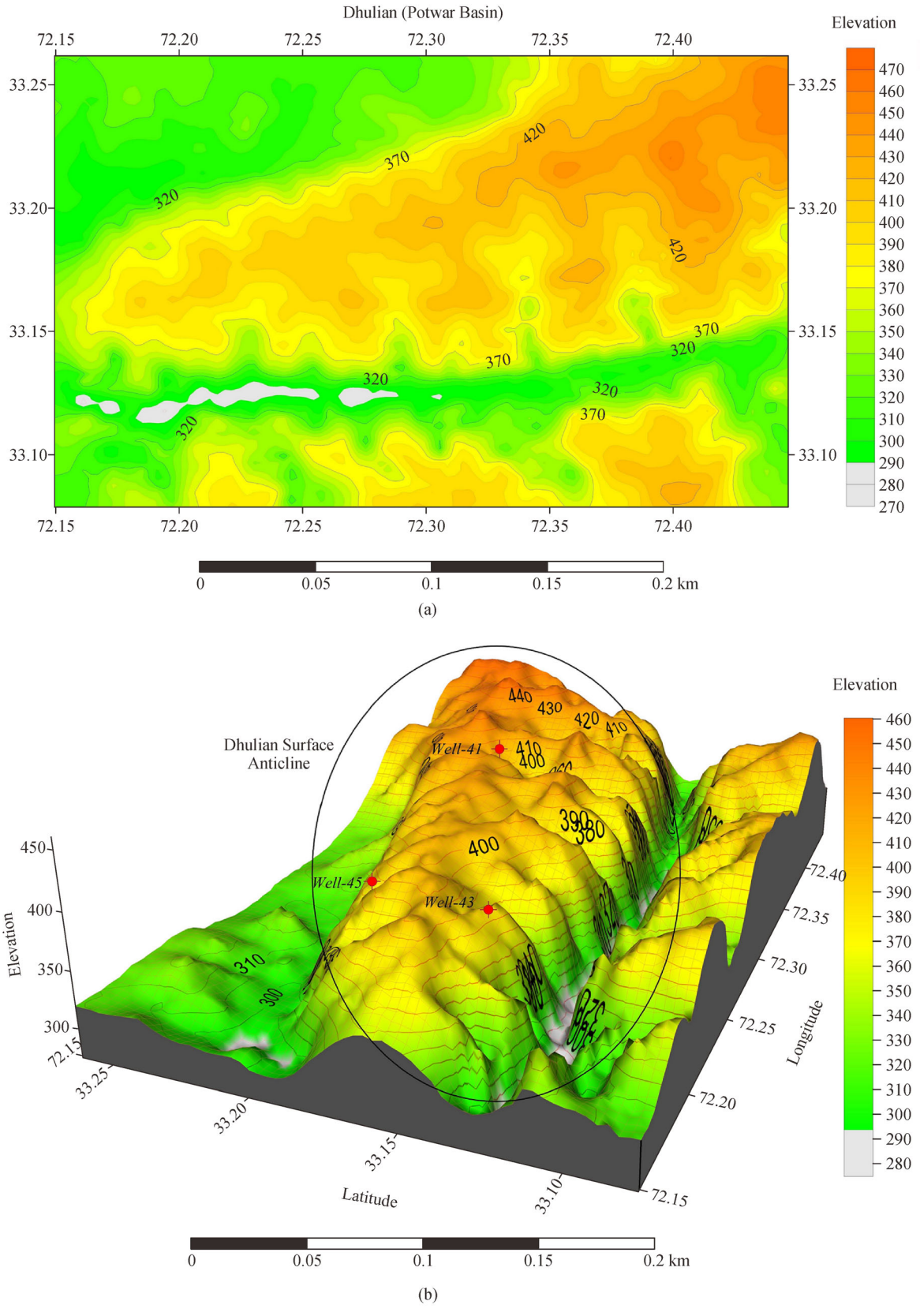

Fig. 6 (a) Two-dimensional and (b) three-dimensional DEM representation of the Dhulian surface structure.

utilized for large-scale basin research because the time-domain or depth-domain features of all seismic lines are utilized to assemble a standard stratum profile (Adeoye and Enikanselu, 2009). The contour lines of each stratigraphic unit in Fig. 7 enable geological structures in the two-way time domain. Two-way time structural contour models of Eocene, Paleocene, early Permian, and Precambrian reflectors with a contour interval of 0.05 s were generated separately. These models demonstrate the geological structural trends in terms of hydrocarbon prospecting and explain the anticlinal structure; therefore, they suggest the hydrocarbon prospects (Fig. 7). The two main faults F1 and F4 are observed in the TWT models, where specific contours are close and form an anticlinal structure. The structure is characterized by the closure of faults on the northward and southward sides and the closure of contours, resulting in a 2way/4way dip closure for hydrocarbon accumulation. Smaller values of the contour plot designate anticlinal structures, and higher values indicate a structurally low area (Fig. 7).

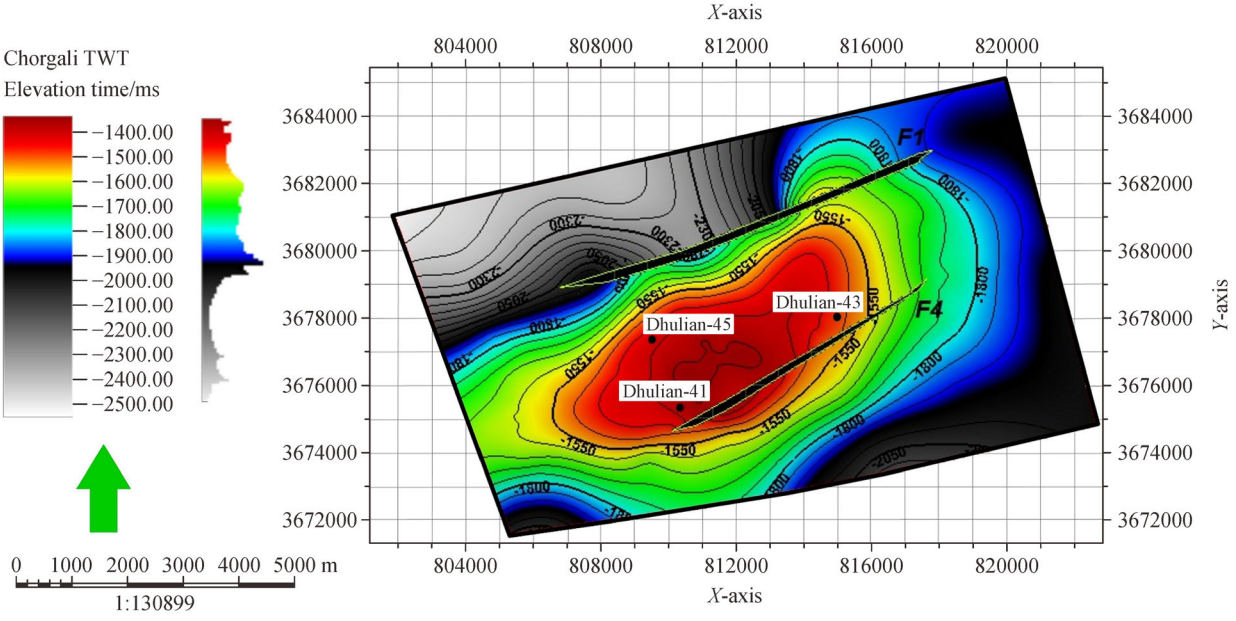

(a)

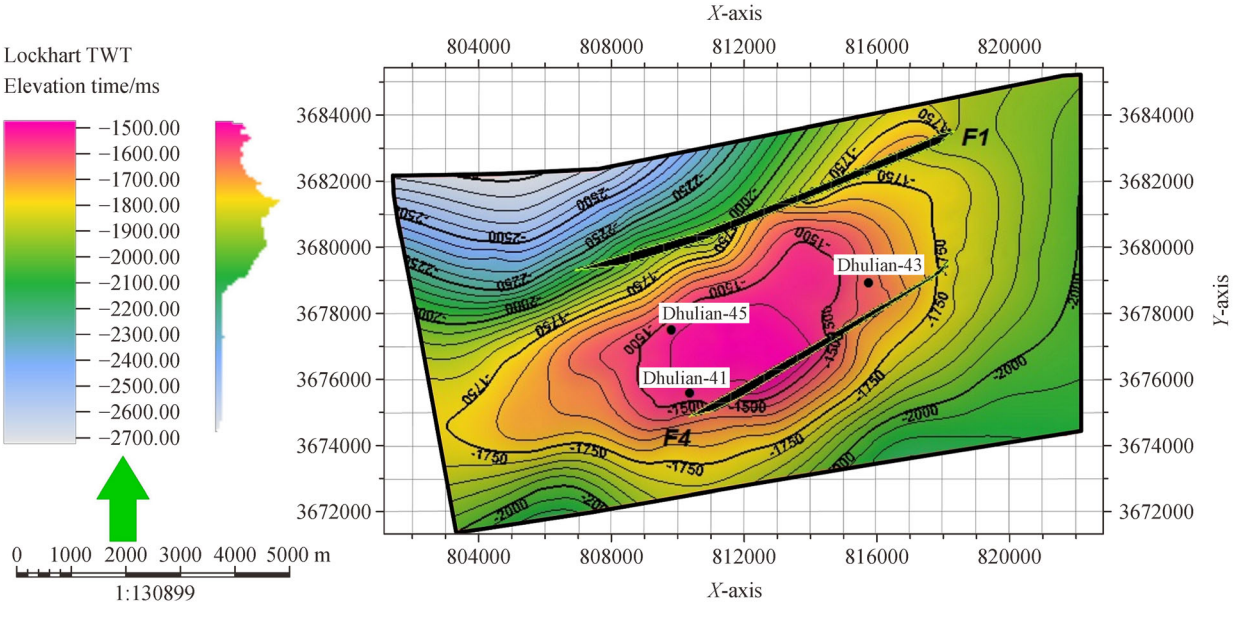

(b)

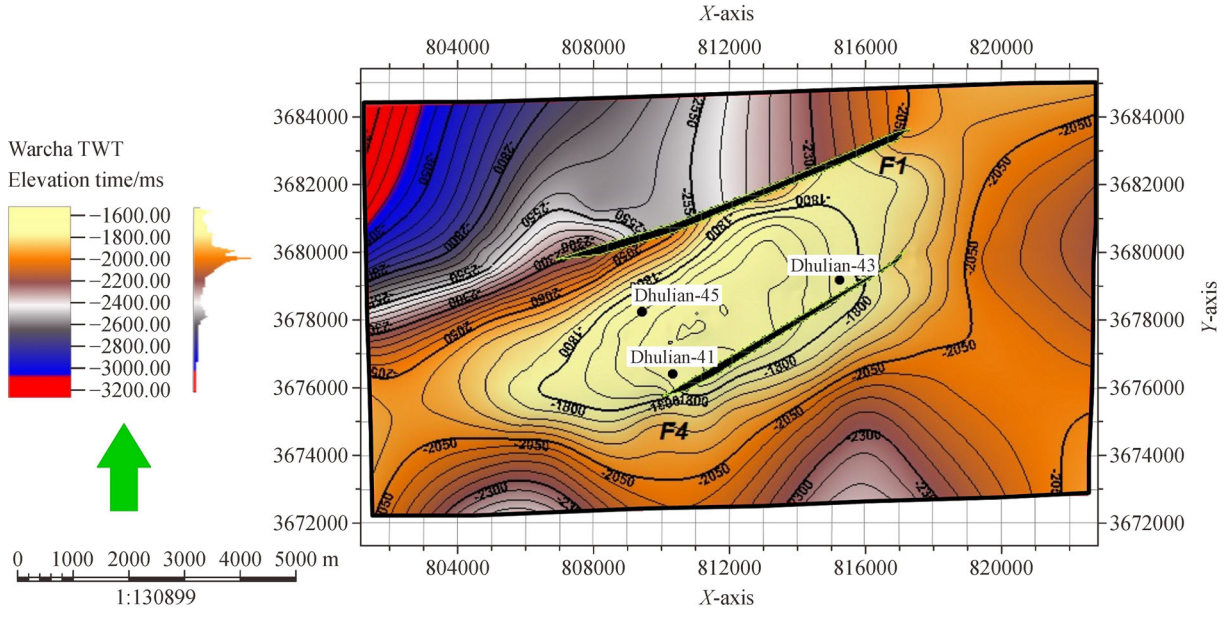

(c)

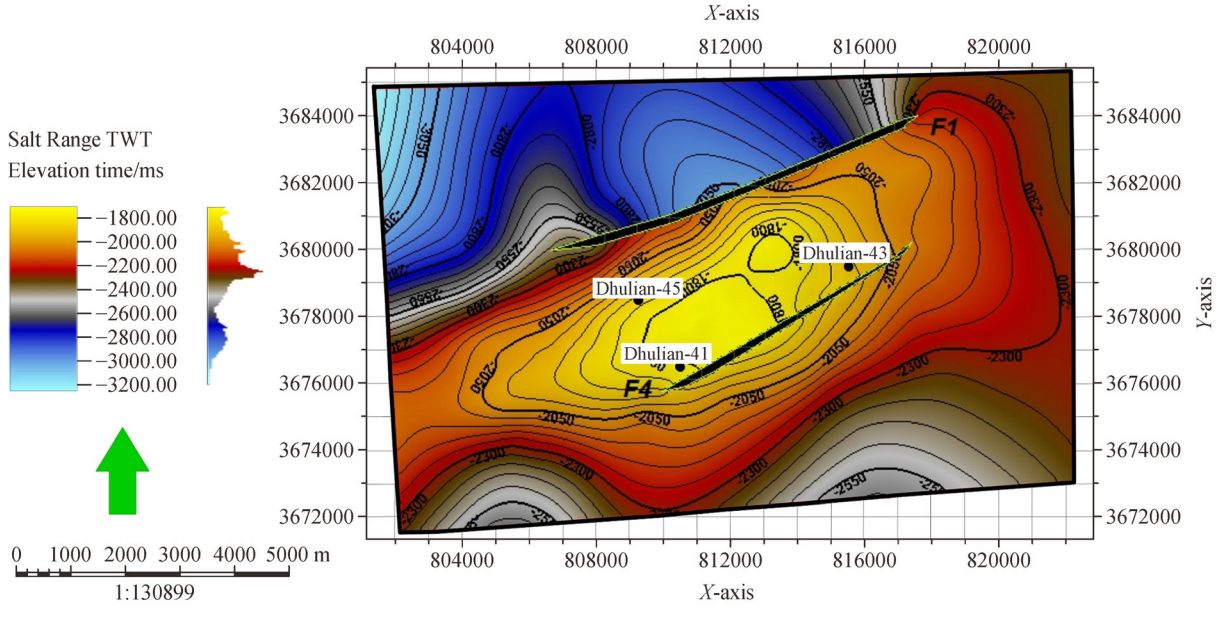

(d)

Fig. 7 Interpreted horizons in TWT represent the 2D TWT contour models of the (a) Chorgali, (b) Lockhart, (c) Warcha, and (d) Salt Range formations. The anticline structure has four-way immersion closure, the center part has a shallow time value, and the reverse fault is NE-SW. The contour interval for all graphics is 3 m. The black dot indicates the location of the well concerning the seismic survey. The mapping projection used for all maps is UTM33.

The depth contour model of the interpreted Chorgali Formation is shown at 50 m contour intervals (Fig. 8(a)). The contour lines range from 2400 to 4200 m. The shallow structure on this model is in the central part of the structure with depth values ranging from 2400 to 2550 m. The depth contour model of the interpreted Lockhart Formation is shown at 50 m contour intervals (Fig. 8(b)). The contour lines range from 3250 to 6000 m. The shallow structure on this model is in the central part of the structure with depth values ranging from 3250 to 3300 m. The depth contour model of the interpreted Warcha Formation is shown at 50 m contour intervals (Fig. 9(a)). The contour lines range from 3250 to 6000 m. The shallow structure on this model is in the central part with depth values ranging from 3250 to 3500 m. The depth contour model of the interpreted Salt Range Formation is shown at 50 m

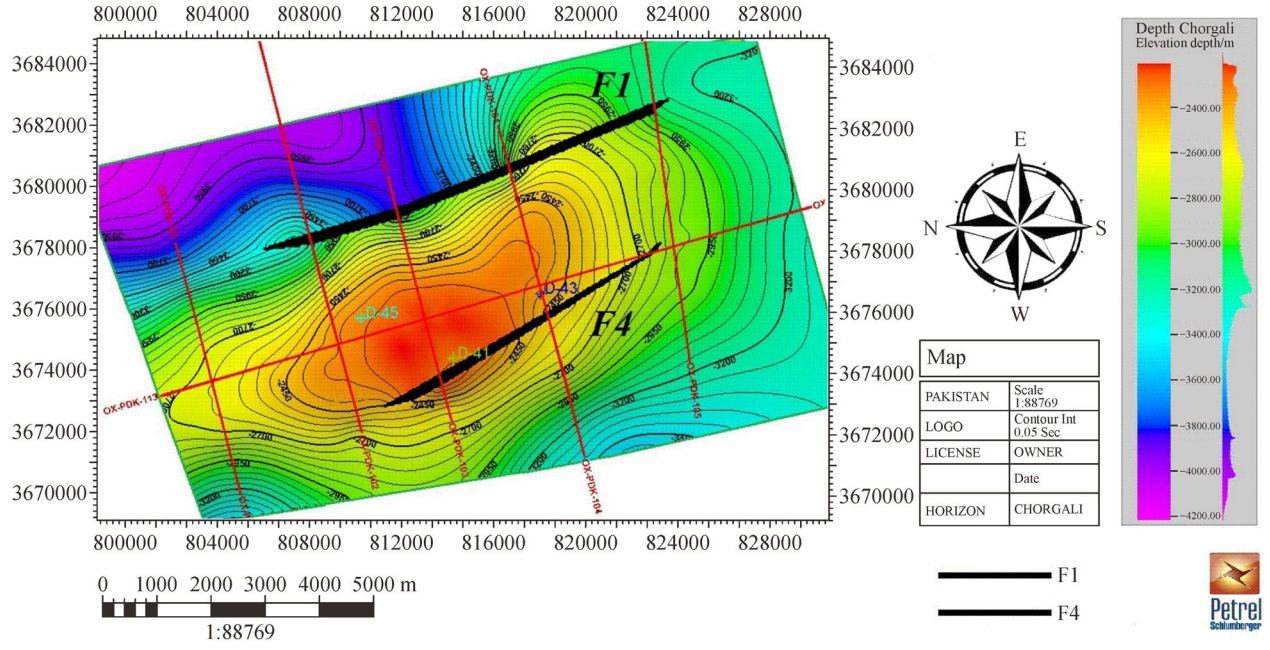

(a)

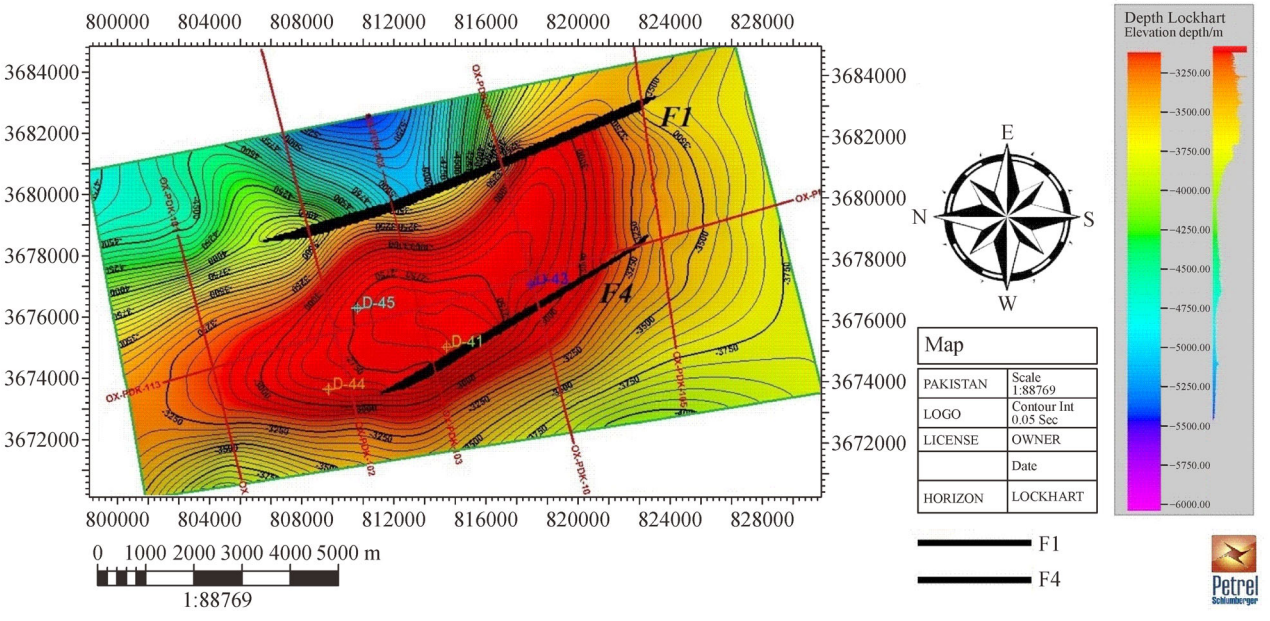

(b)

Fig. 8 2D depth contour models of the (a) top Eocene limestone Chorgali Formation and (b) upper Paleocene limestone Lockhart Formation, where the shallow depths in the central part of the surface designate the Dhulian anticlinal structure with four-way dip closure.

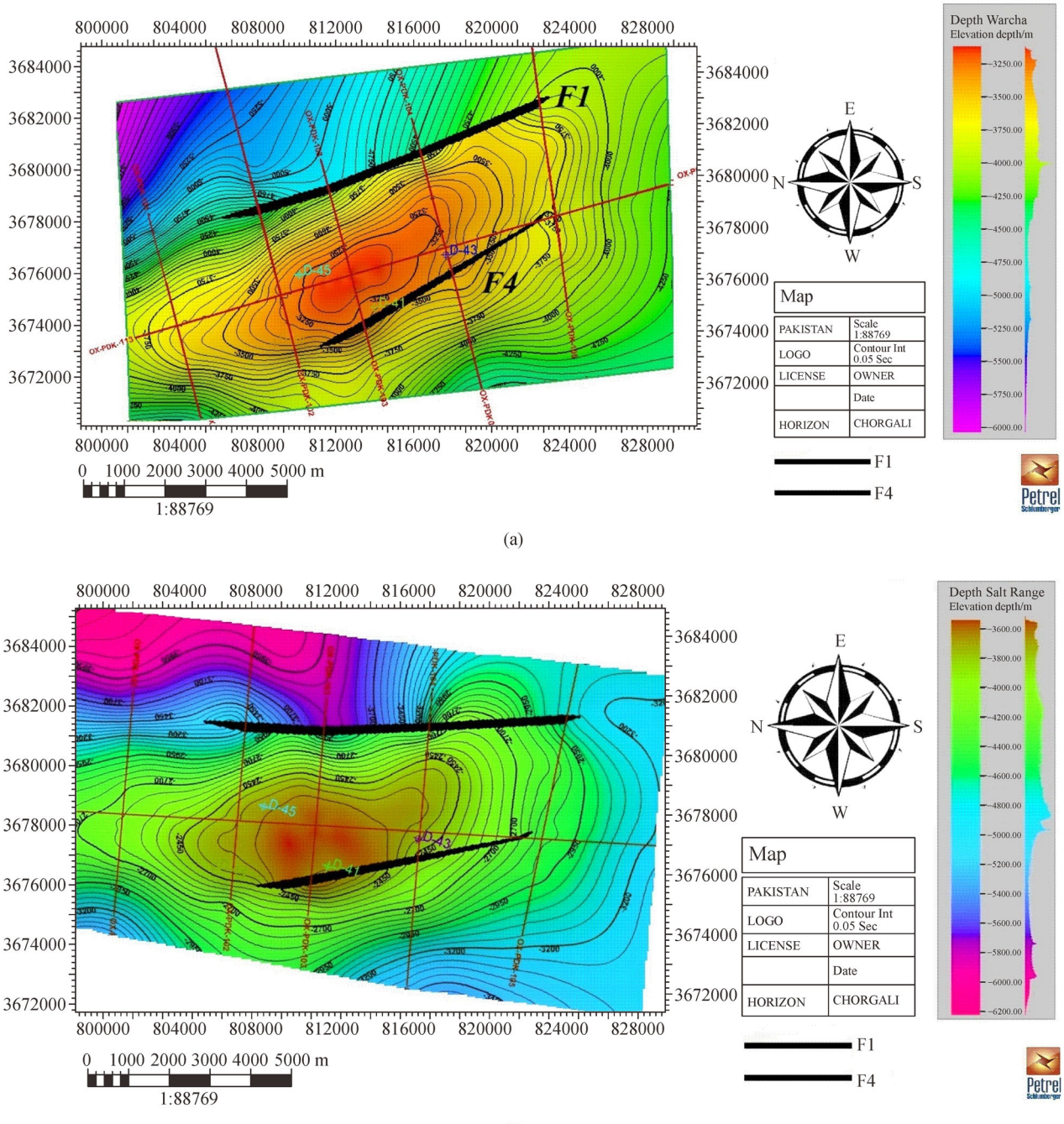

Fig. 9 2D depth contour models of the (a) early Permian arkosic sandstone Warcha Formation and (b) Precambrian Salt Range Formation, where the shallow depths in the central part of the surface designate the Dhulian anticlinal structure with four-way dip closure.

contour intervals (Fig. 9(b)). The contour lines range from 3600 to 6200 m. The shallow structure on this model is in the central part with depth values ranging from 3600 to 3750 m. These depth contour models display a NE to SW (fold axis) broadened anticline structure bounded by two faults (F1 and F4) on its limbs, which is responsible for the accumulation of hydrocarbons. The crest is high in the structure; consequently, it designates the possible presence of hydrocarbons.

4.3 3D structural model

Geophysical and geological data are the basic information for building high-precision 3D geological models. The

structure and formation characteristics of geological objects are essential factors underlying the production of hydrocarbons (Mehmood et al., 2016; Guo et al., 2017). One of the key challenges in reservoir modeling is the accurate representation of reservoir geometry, including the structural framework (i.e., horizons/major depositional surfaces, and fault surfaces) and detailed stratigraphic layers. The structural frameworks delineate major compartments of a reservoir and often provide first-order controls on in-place fluid volumes and fluid movement during production. 3D structural models of the Eocene limestone Chorgali, upper Paleocene limestone Lockhart, early Permian arkosic sandstone Warcha, and Precambrian Salt Range formations ultimately show the anticline structural framework of the Dhulian oilfield. Riaz et al. (2019) proved the existence of thrusting and anticline structure elongated with two major reverse faults, dipping towards each other, in the Potwar basin, and confirmed the tectonic compression in this area. Therefore, in this study, based on 3D Petrel structural modeling, the evaluation and development of reservoir indexes, such as the true 3D reservoir structure trend, slope, channel characteristics, geometry type, depth, and hydrocarbon prospect possibility, were determined.

The two-way time isochrones of the Chorgali, Lockhart, Warcha and Salt Range formations range from 1400–2500 ms, 1500–2700 ms, 1600–3200 ms, and 1800–3200 ms, respectively. The contour lines directly reflect the change in the formations with depth (Figs. 10–13). Based on the combined set of seismic reflection and geophysical well log data, the 3D structural analysis and interpretation concluded that all 3D models have complex structural trends. The stratigraphic units include the Eocene limestone Chorgali, upper Paleocene limestone Lockhart, early Permian arkosic sandstone Warcha, and Precambrian Salt Range formations with complicated broadened salt cored anticline (10°–20°) structures. The vertical axis of the anticline tends to the northeast to southwest, and continues to shrink to the northeast, which confirms that the region is postulated to be in compression mode and has the possibility of hydrocarbons. The crests of all models are high in the structure; consequently, and it designates the possible presence of hydrocarbons. Moreover, the petrophysical analysis also demonstrates that the hydrocarbon saturation in the two reservoirs is sufficient and indirectly reflects the efficiency of the established 3D structural model in this study.

In future work, to reveal the valuable hidden horizons on the seismic reflection profiles, actual 3D stratigraphic solid modeling integrating multisource data constraints (Guo et al., 2018) and uncertainty evaluation of 3D structural model (Wellmann et al., 2018) should be carried out.

4.4 Seismic attribute analysis

Seismic attributes are described as implicit calculated and measured quantities derived from seismic data (Taner, 2001). Compared with conventional methods of interpreting seismic stratigraphy, seismic attributes provide useful information about the amplitude, location, and shape of

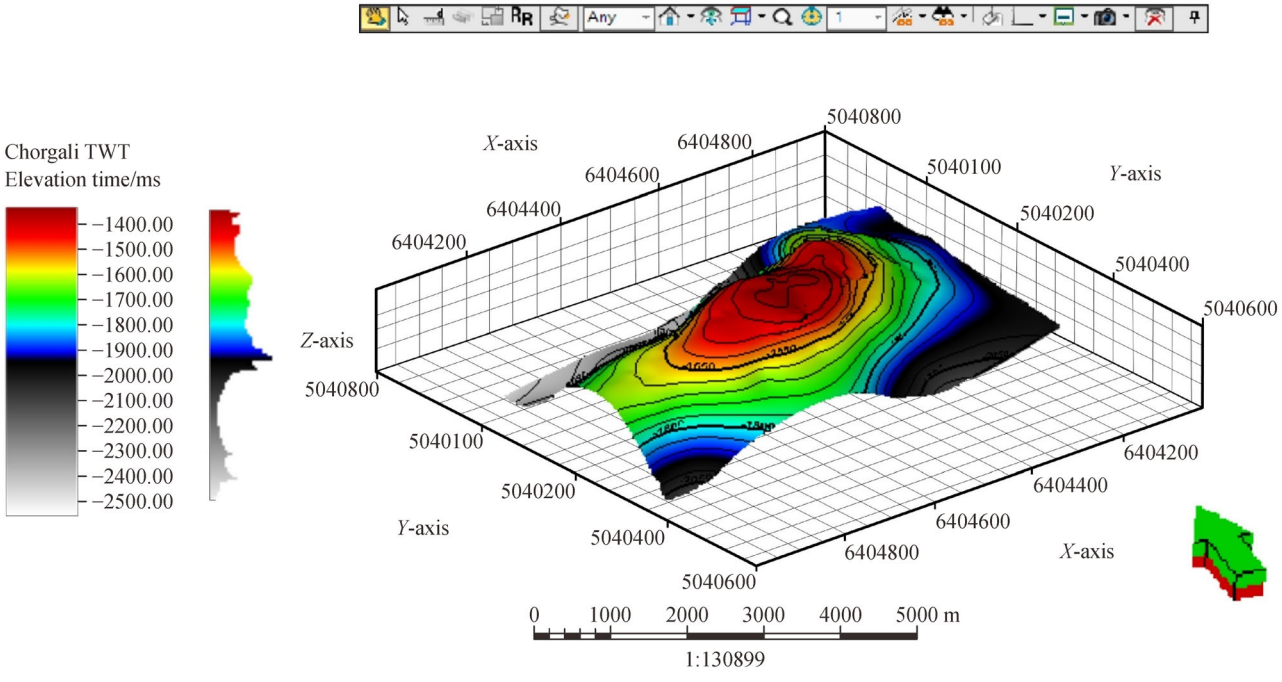

Fig. 10 3D structural model of the top Eocene limestone Chorgali Formation.

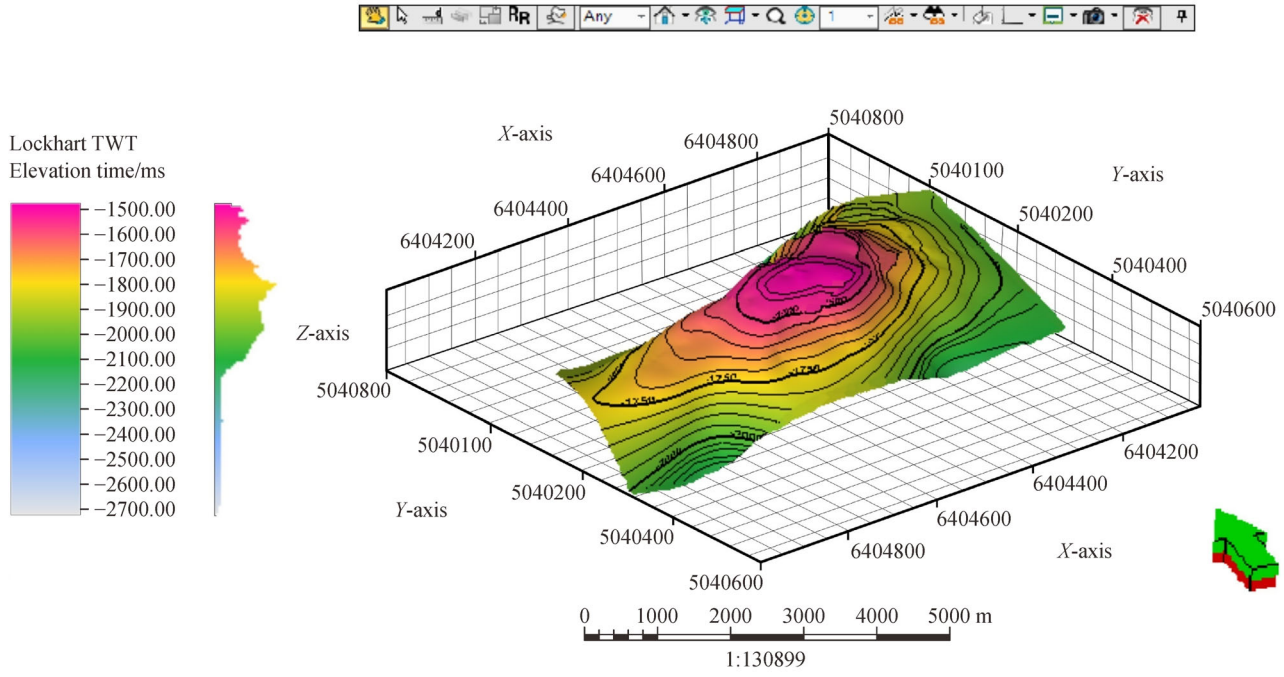

Fig. 11 3D structural model of the top upper Paleocene limestone Lockhart Formation.

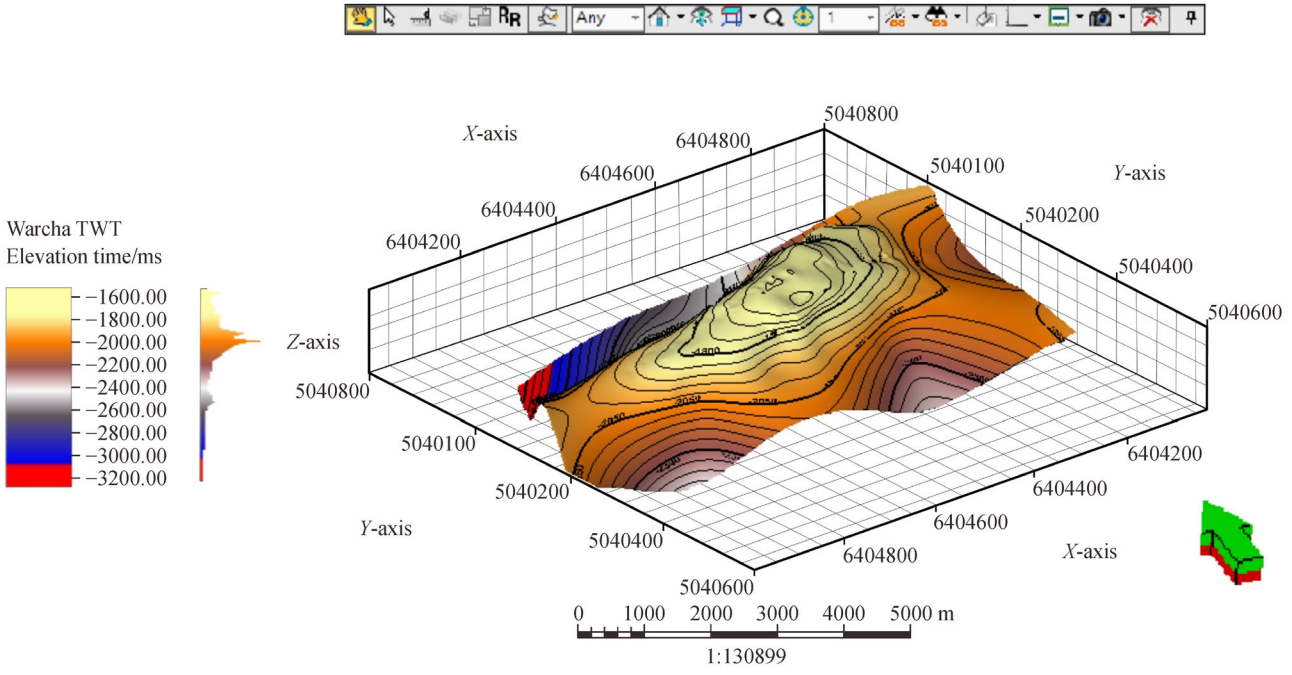

Fig. 12 3D structural model of the top early Permian arkosic sandstone Warcha Formation.

seismic waveforms. Therefore, this information is important qualitative or quantitative predictive factor for reservoir characteristics and geometric prediction. Due to the complex horizontal and vertical geometrical distribution, it is not always possible to predict the geometric distribution of reservoirs based on conventional seismic interpretation. Therefore, to better understand the spatial predictions of the subsurface structure, formation extrusion, and reflector continuity, this study utilized several various seismic attributes, e.g., trace envelope (instanta-

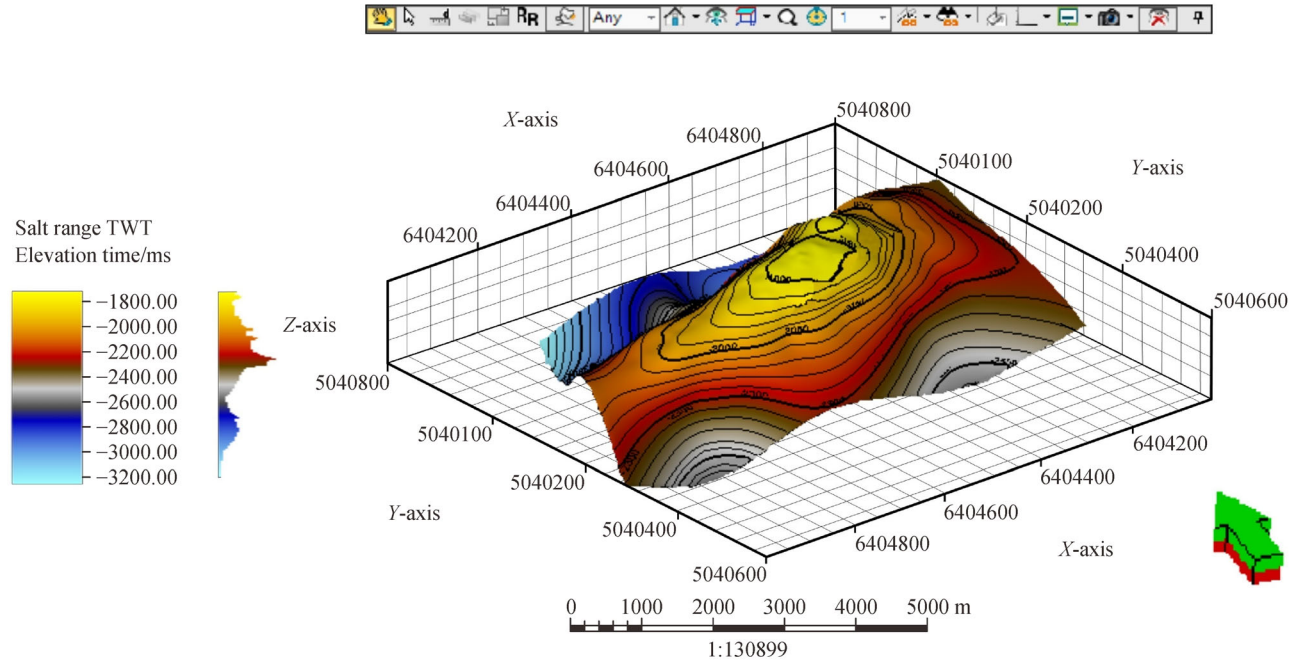

Fig. 13 3D structural model of the top Precambrian saline series Salt Range Formation.

neous amplitude), instantaneous frequency, and average energy. The trace envelope attribute shows changes in lithology and thin-bed tuning effects. In contrast, the instantaneous frequency attribute designates the hydrocarbon bearing zone, fracture zones, formation thickness, and average energy attribute, and they represent the reflection intensity and lateral continuity of the reflector.

4.4.1 Trace envelop (instantaneous amplitude)

The trace envelope attribute is a physical attribute that represents an effective discriminator for sequence boundaries, thin-bed tuning effects, major changes in the depositional environment, etc. Physical attributes are related to physical qualities and quantities. The magnitude of the trace envelope is generally proportional to the acoustic impedance contrast through lithological contact (Barnes, 1991). The lithological contact between shale and limestone produces high acoustic impedance because limestone has higher density and velocity than shale (Fig. 14(a)). Accordingly, a high amplitude value is perceived across the lithological contact boundary. The envelope trace of seismic line OX-PDK-104 shows the main changes in lithology. High reflection intensities were detected at the level of the Chorgali Formation, which confirms the presence of dense lithologies. However, the Lockhart and Warcha formations are more valuable than the Chorgali Formation due to the compactness of limestone. Weak reflections are due to the interlacing of shale. Despite negative reflection coefficients, limestone formations that dominate clay formations produce a positive response in this attribute. In this study, the trace envelope amplitude reveals the intensity of the reflection to facilitate the interpretation of horizons and faults, especially small faults. The prevalence of the high amplitude values across the lithological contact boundary reveals the presence of dense lithology. The trace envelope attribute can also be used to identify major changes in the sedimentary or lithological environment, which will facilitate spatial correlations with porosity.

4.4.2 Instantaneous frequency

The instantaneous frequency attribute responds to both wave propagation effects and depositional characteristics. Hence, in this study instantaneous frequency attributes are considered as physical attributes and used as effective discriminators including low-frequency anomalies as hydrocarbon indicators and high-frequency anomalies as bed thickness indicators. Limestone shows high frequency as a sharp interface, such as thin shale specified by the higher frequency (Fig. 14(b)). In the reservoir, the lower frequency indicates the presence of hydrocarbons. Accordingly, due to the oil content in the pores, sand or limestone sometimes exacerbates this low frequency anomaly. Within the area of the reservoir, patches of lower frequencies indicate the presence of hydrocarbons. In the Chorgali and Lockhart formations, the limestone shows a relatively high frequency. Due to the presence of shale, higher frequency values were observed above the reservoir (Fig. 14(b)).

4.4.3 Average energy

The average energy attribute of seismic waves is a measure of reflectivity in the specified time window. According to the above description, the higher the potential energy, the higher the amplitude. A compact lithology exhibits high energy, while a loose lithology exhibits low energy values (Chen and Sidney, 1997). The average energy attribute also delineates the reservoir quality. The continuity of reflectors at the level of the Chorgali and Lockhart formations can be seen using this attribute (Fig. 14(c)). The high energy content of the Chorgali and Lockhart formations is attributed to the high reflection intensity of limestone. The average energy applied to the seismic line indicates that the continuity of the reflector is more apparent than an average seismic profile (Fig. 14(c)). High energy is also a sign of good reservoir quality. The presence of shale leads to low energy above and below the reservoir. The response energy also characterizes acoustic rock properties and bed thicknesses. The average energy is often strongly correlated with liquid saturation (oil/water vs. gas) because it has a strong effect on both velocity and density. While the energy of seismic reflections is generated at boundaries where the acoustic impedance (the production of velocity and density) changes.

4.5 Petrophysical properties

After identifying the geometry of the stratigraphic units, the petrophysical properties of the top Eocene limestone Chorgali Formation and upper Paleocene limestone Lockhart Formation were identified (Figs. 15–17). The calculated petrophysical parameters of the Eocene limestone Chorgali Formation and upper Paleocene limestone Lockhart Formation along the three wells are shown in Tables 1 and 2. The overall description of any reservoir depends on these petrophysical parameters. Shale volume is an indicator of the status and condition of the reservoir (a smaller the shale volume corresponds to better the reservoir quality). In all wells, porosity values difference, depth variation, and permeability changes can be seen in the Eocene limestone Chorgali Formation and upper Paleocene limestone Lockhart Formation (Tables 1 and 2). All wells have good porosity as indicated by Rider (Everett et al., 2002). The permeability of both reservoirs is higher than 1000 MD in all wells. Among them, the permeability of the Chorgali reservoir is high in well 43, and the Lockhart reservoir permeability is high in well 41. The application of the previously derived petrophysical parameters was used to predict the saturation of the reservoir, which designates the hydrocarbon prospects of the reservoir. The highest net to gross ratio of the Chorgali Reservoir is penetrated by well 43, However, the Lockhart Reservoir has the highest net to gross ratio in well 41. Based on the petrophysical parameters in each well, the average petrophysical properties are calculated for the two reservoirs (Table 3, Figs. 18 and 19). Awais et al. (2019) characterized the Chorgali Reservoir using integrated seismic and logging data and determined the properties of the Chorgali Formation, which are similar to our results.

4.6 Hydrocarbon evaluation

The hydrocarbon volumetric calculation needs static reservoir properties, such as lithology, permeability, fluid saturation, net to gross ratio, thickness of reservoir and porosity. The overall description of the reservoir depends on these petrophysical characteristics, which is of great significance in determining whether the reservoir is economically practical or not. The volumetric calculation method has been applied, which integrates the reservoir properties calculated via previous petrophysical analysis. The results show that in all Dhulian wells, the Eocene limestone Chorgali and upper Paleocene limestone Lockhart formations show good hydrocarbon saturation (Fig. 20). Therefore, the Chorgali and Lockhart reservoirs are considered to be economically viable reservoirs. Table 3 summarizes the average petrophysical properties, and the volumetric formula reveals that the stock tank oil in place in million stock tank barrels (MMSTB) accounts for 74.87% (MMSTB) in the Chorgali Formation and 67.56% (MMSTB) in the Lockhart Formation.

5 Conclusions

The results indicate that the Dhulian three-dimensional surface structure is a virtually symmetrical anticline with a maximum dip of 30° to 35°, which confirms that the region is postulated to be in compression mode. Seismic interpretation based synthetic seismograms recognized four seismic horizons, normal faults, and anticlines structures bounded by two reverse faults on both limbs in the covered sequence. These two main reverse faults have a fold axis trend from ENE to WSW. Based on reflection terminations and seismic reflector observations in terms of their amplitude, continuity, configuration, frequency and corresponding external geometries, four major sequences were observed. Structural and lithological interpretations were also revealed through seismic attribute maps (i.e., envelopes, instantaneous phases, and average energy), which magnified the structure, strata, and spatial predictions of the subsurface structure, formation extrusion, and reflector continuity. Petrel structural modeling workflow, which includes the steps of fault modeling, pillar meshing, and vertical layering represents a useful method for understanding the three-dimensional structure of reservoirs. Hence, 3D structural models of four mapped reservoirs demonstrate a NE to SW (fold axis) broadened anticline structure. A high crest in the structure indicates the possibility of hydrocarbons. Based on the qualitative analysis of the petrophysical parameters, reservoir

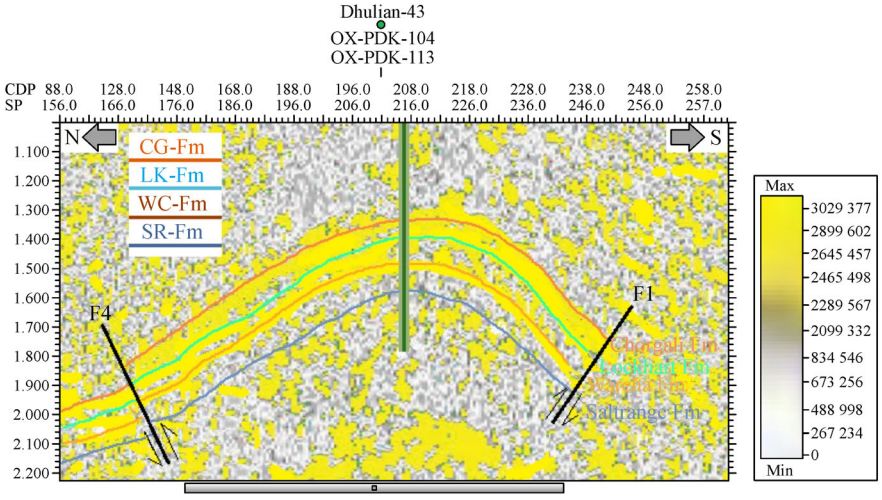

(a)

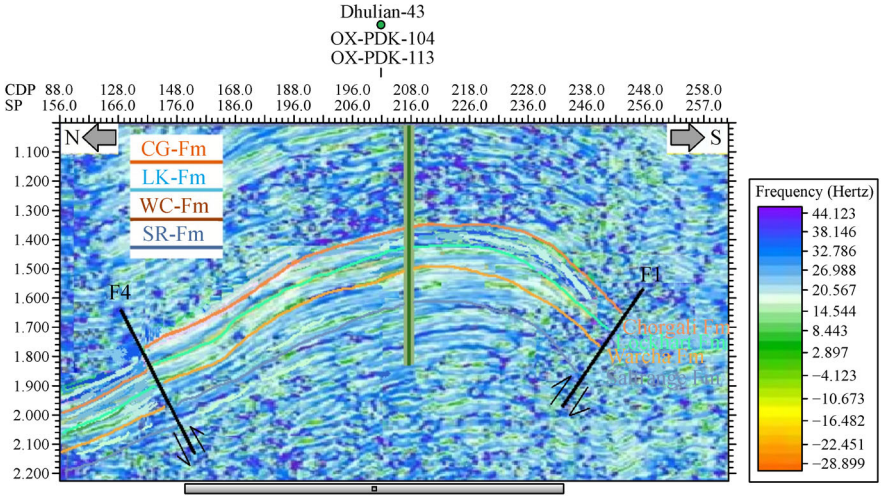

(b)

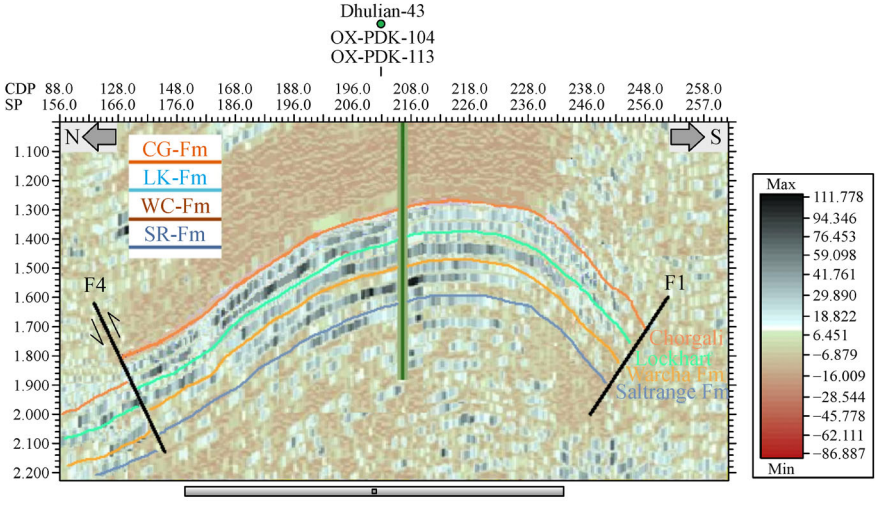

(c)

Fig. 14 (a) Envelope attribute map, (b) frequency attribute map, and (c) average energy attribute map of the OX-PDK-104 seismic line [Chorgali (red), Lockhart (green), Warcha (pink), Salt Range (blue)].

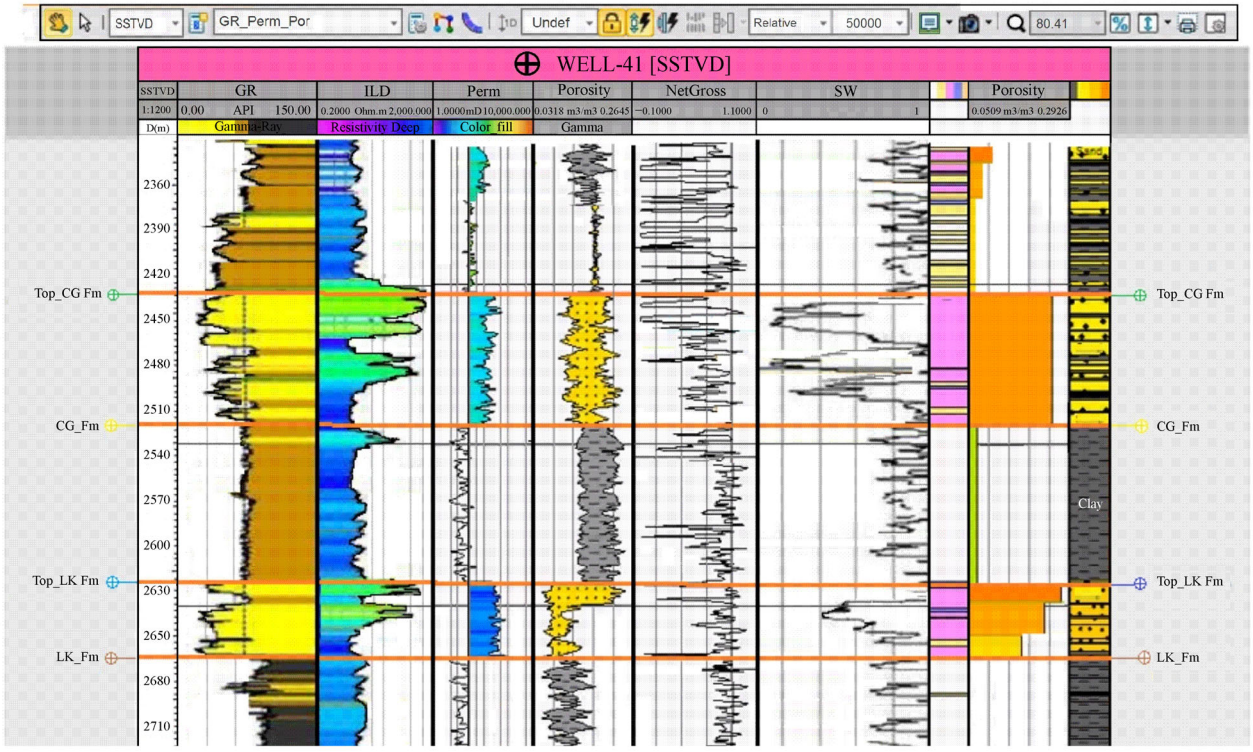

Fig. 15 Wireline log signature and derived petrophysical characteristics of the Chorgali (CG) and Lockhart (LK) formations in well 41.

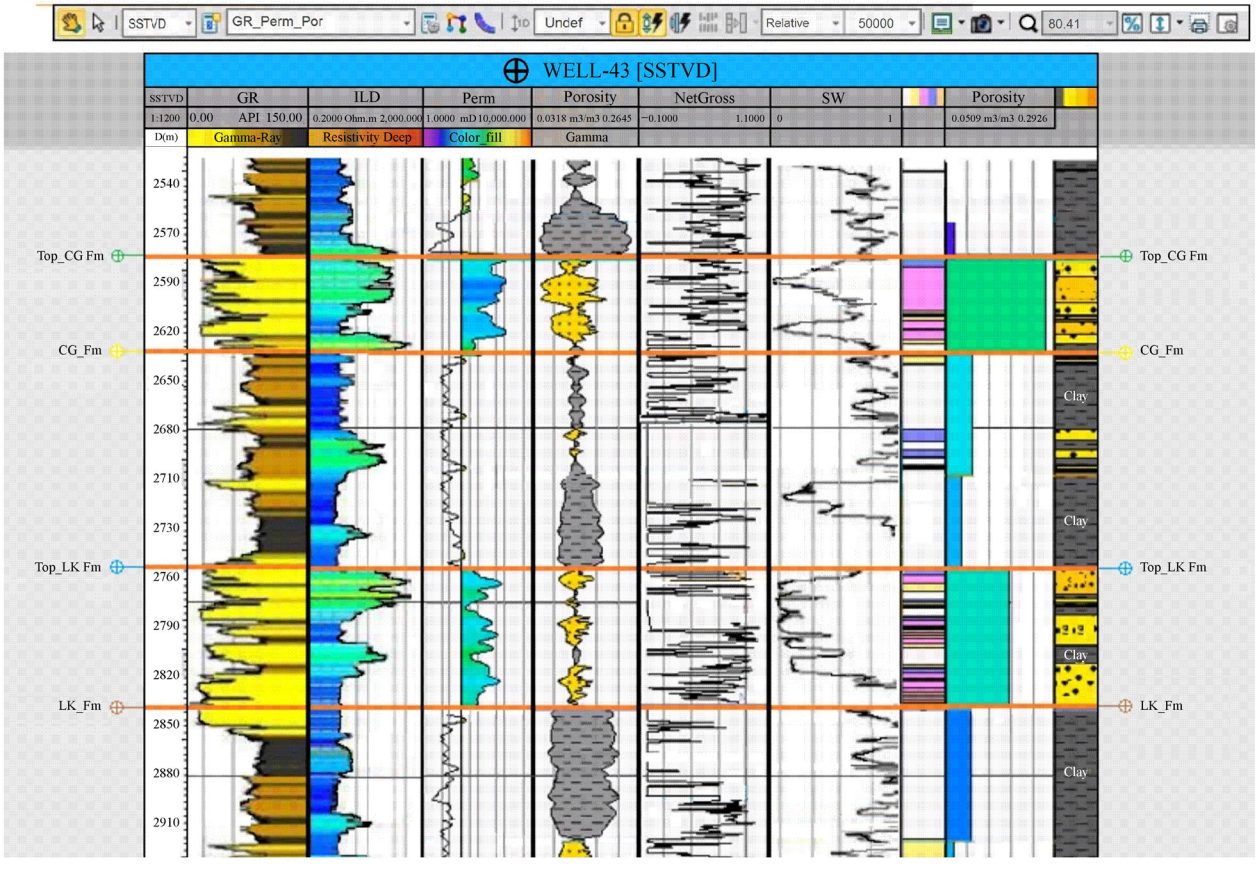

Fig. 16 Wireline log signature and derived petrophysical characteristics of the Chorgali (CG) and Lockhart (LK) formations in well 43.

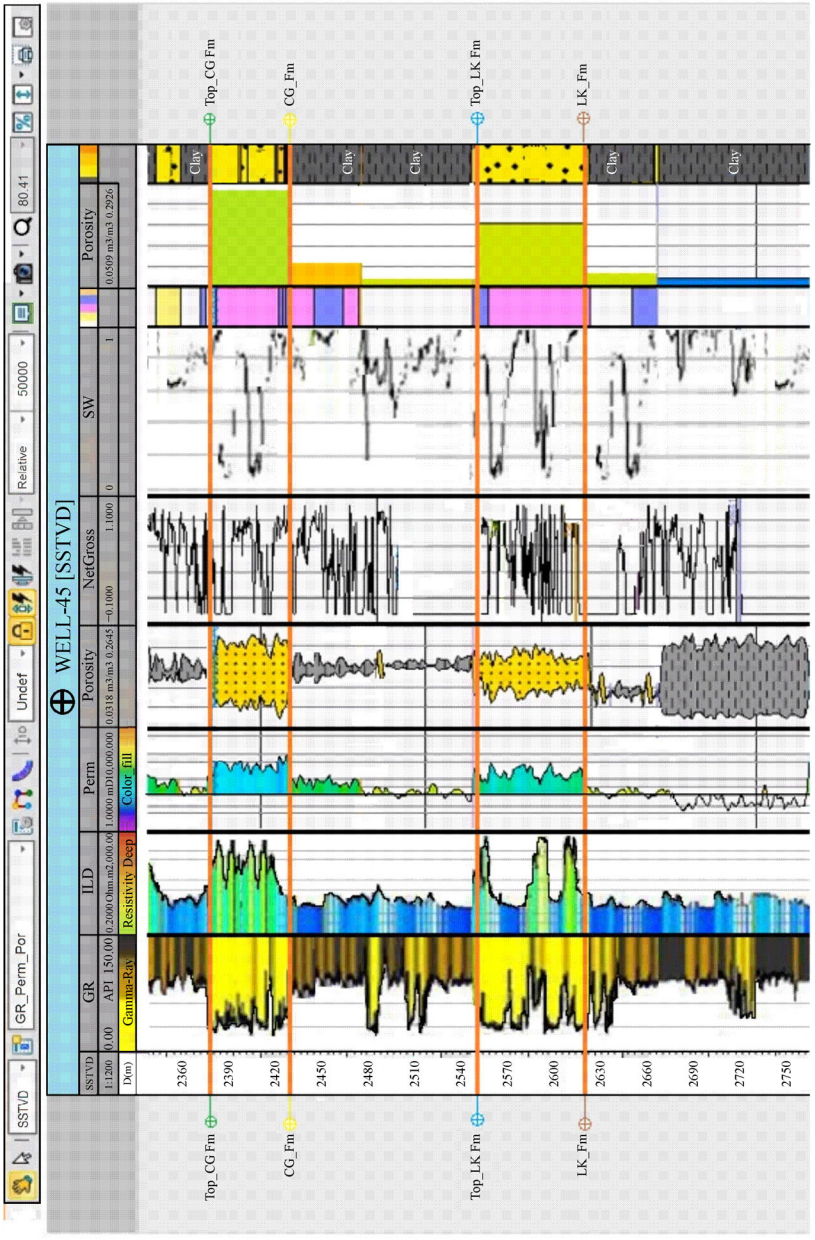

Fig. 17 Wireline log signature and derived petrophysical characteristics of the Chorgali (CG) and Lockhart (LK) formations in well 45.

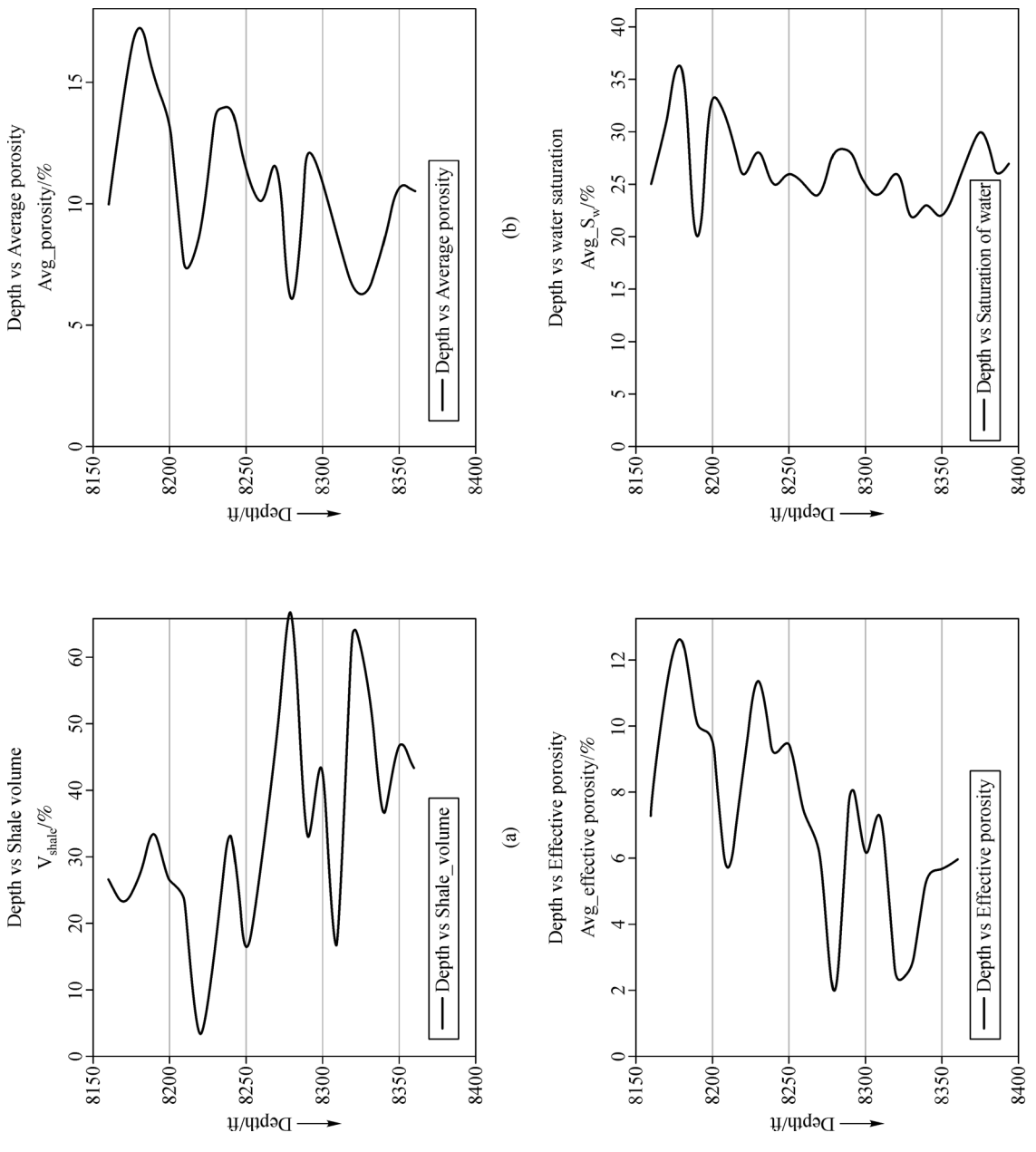

Fig. 18 Petrophysical properties of the Chorgali Formation: (a) volume of shale, (b) average porosity, (c) average effective porosity, and (d) water saturation as a percentage.

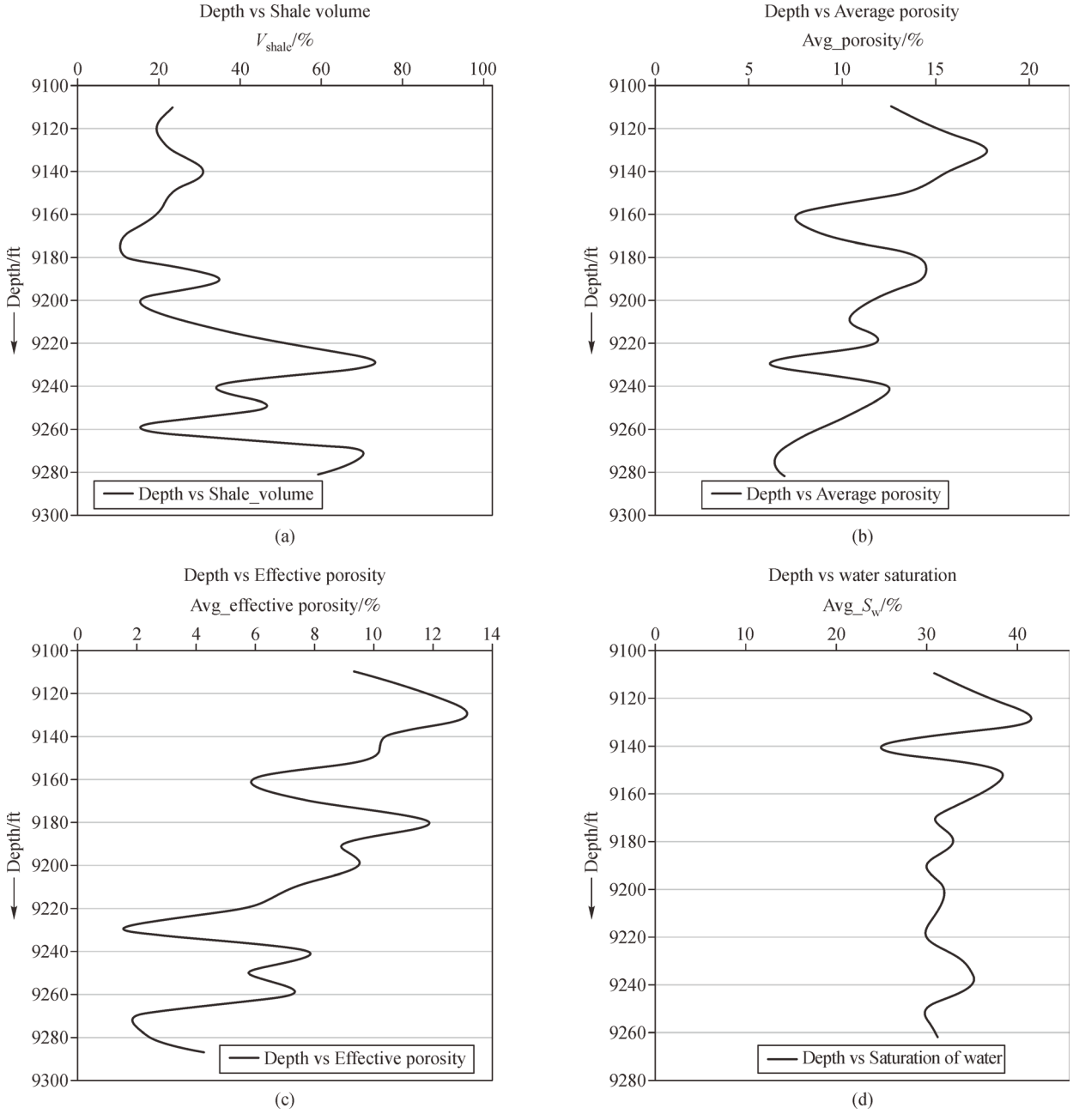

Fig. 19 Petrophysical properties of the Lockhart Formation: (a) volume of shale, (b) average porosity, (c) average effective porosity, and (d) water saturation as a percentage.

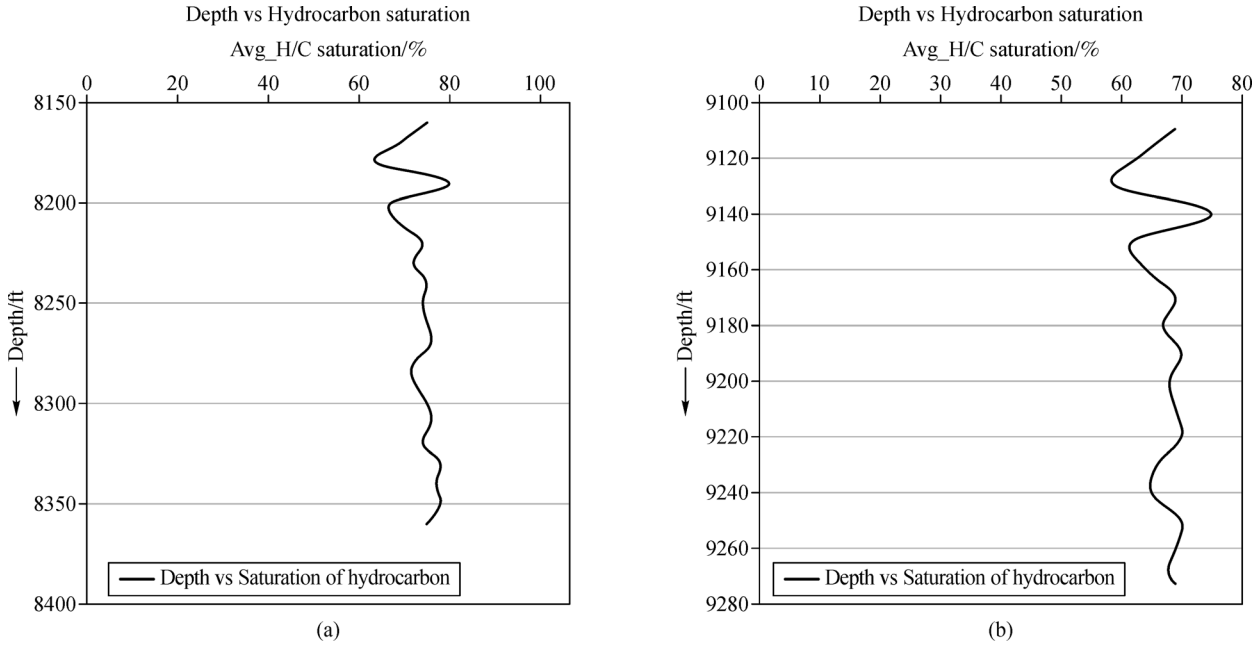

Fig. 20 Hydrocarbon saturation (%) of the (a) Chorgali Formation (CG) and (b) Lockhart Formation (LK).

Table 1 Summary of petrophysical properties estimated from wireline logs for the Chorgali (CG) Formation

Reservoir parameters	Well-41	Well-43	Well-45
Lithology	Eocene-Limestone	Eocene-Limestone	Eocene-Limestone
Formation interval (m)	2430.22−2510	2577−2633.33	2375.74−2427
Net thickness (ft)	130	140	126
V_{Shale}[a] (Fraction)	0.16	0.18	0.22
K[b] (md)	1140.14	1312.75	1020.87
Avg. Φ[c] (%)	12.98	17.34	14.96
Effective Φ (%)	8.35	10.00	9.88
Avg. S_w[d] (Fraction)	0.28	0.26	0.32
NTG[e] (Fraction)	0.61	0.78	0.48

Notes: a) V_{Shale}: volume of shale; b) K: permeability; c) Avg. Φ: average porosity; d) Avg. S_w: average water saturation; and e) NTG: net to gross ratio.

Table 2 Summary of petrophysical properties estimated from wireline logs for the Lockhart (LK) Formation

Reservoir parameters	Well-41	Well-43	Well-45
Lithology	Paleocene-Limestone	Paleocene-Limestone	Paleocene-Limestone
Formation interval (m)	2620.59−2670	2755−2835.43	2545−2620.56
Net thickness (ft)	118.66	90	120
V_{Shale}[a] (Fraction)	0.12	0.20	0.16
K[b] (md)	1003.90	1123.00	1245.02
Avg. Φ[c] (Fraction)	11.78	16.34	12.96
Effective Φ (%)	11.15	11.15	11.15
Avg. S_w[d] (Fraction)	0.46	0.22	0.09
NTG[e] (Fraction)	0.56	0.70	0.88

Notes: a) V_{Shale}: volume of shale; b) K: permeability; c) Avg. Φ: average porosity; d) Avg. S_w: average water saturation; and e) NTG: net to gross ratio.

Table 3 Average petrophysical properties in all wells and total STOIIP (MMSTB).

Reservoir	Average petrophysical parameters				
	Porosity/%	*K*/md	S_w/Fraction	NTG/%	STOIIP [a] (MMSTB)
CG	15.09	1157	0.28	0.78	73.66
LK	13.69	1123	0.25	0.71	57.14

Note: a) STOIIP: stock tank oil in place

properties, including the porosity, permeability, net pay thickness, water saturation, and hydrocarbon saturation, were calculated for the Eocene limestone Chorgali and upper Paleocene limestone Lockhart reservoirs. The results show that all wells of both reservoirs have high quality and display good hydrocarbon saturation; therefore, these formations are considered economically viable reservoirs.

Acknowledgements This study was supported by grants from the National Natural Science Foundation of China (Grant Nos. 42072326 and 41772348) and the National Key Research and Development Program of China (Nos. 2019YFC1805905 and 2017YFC0601503).

References

Aamir M, Siddiqui M M (2006). Interpretation and visualization of thrust sheets in a triangle zone in eastern Potwar, Pakistan. Leading Edge (Tulsa Okla), 25(1): 24–37

Adeoye T, Enikanselu P (2009). Hydrocarbon reservoir mapping and volumetric analysis using seismic and borehole data over "Extreme"-field, southwestern Niger Delta. Ozean J Appl Sci, 2(4): 429–441

Aguilera R F, Aguilera R (2004). A triple porosity model for petrophysical analysis of naturally fractured reservoirs. Petrophys, 45(02): 157–166

Ameloko A, Owoseni A (2015). Hydrocarbon reservoir evaluation of X-field, Niger Delta using seismic and petrophysical data. Inter J Innov Scient Res, 15(1): 193–201

Archie G E (1942). The electrical resistivity log as an aid in determining some reservoir characteristics. Transact AIME, 146(01): 54–62

Asquith G, Krygowski D (2004). AAPG Methods in Exploration, No. 16, Chapter 7: Log Interpretation

Awais M, Hanif M, Khan M Y, Jan I U, Ishaq M (2019). Relating petrophysical parameters to petrographic interpretations in carbonates of the Chorgali Formation, Potwar Plateau, Pakistan. Carbonates Evaporites, 34(3): 581–595

Baker D M, Lillie R J, Yeats R S, Johnson G D, Yousuf M, Zamin A S H (1988). Development of the Himalayan frontal thrust zone: Salt Range, Pakistan. Geology, 16(1): 3–7

Barnes A E (1991). Instantaneous frequency and amplitude at the envelope peak of a constant-phase wavelet. Geophys, 56(7): 1058–1060

Bitrus P R, Iacopini D, Bond C E (2016). Defining the 3D geometry of thin shale units in the Sleipner reservoir using seismic attributes. Mar Pet Geol, 78: 405–425

Blythe A, Burbank D, Farley K, Fielding E (2000). Structural and topographic evolution of the central Transverse Ranges, California, from apatite fissiontrack,(U–Th)/He and digital elevation model analyses. Basin Res, 12(2): 97–114

Burrough P A, McDonnell R, McDonnell R A, Lloyd C D 2015. Principles of Geographical Information Systems. Oxford: Oxford University Press

Butler R W, Coward M P, Harwood G M, Knipe R J (1987). Salt control on thrust geometry, structural style and gravitational collapse along the Himalayan mountain front in the Salt Range of northern Pakistan. In: Lerche, J.J. O'Brien, eds. Dynamical Geology of Salt and Related Structures. New York: Elsevier: 339–418

Chen N, Ni N, Kapp P, Chen J, Xiao A, Li H (2015). Structural analysis of the Hero Range in the Qaidam Basin, northwestern China, using integrated UAV, terrestrial LiDAR, Landsat 8, and 3-D seismic data. IEEE J Sel Top Appl Earth Obs Remote Sens, 8(9): 4581–4591

Chen Q, Sidney S (1997). Seismic attribute technology for reservoir forecasting and monitoring. Leading Edge (Tulsa Okla), 16(5): 445–448 (J)

Dowd P (1994). Geological controls in the geostatistical simulation of hydrocarbon reservoirs. Arabian J Sci Eng, 19(2B): 237–247

Ehsan M, Gu H, Ahmad Z, Akhtar M M, Abbasi S S (2019). A modified approach for volumetric evaluation of shaly sand formations from conventional well logs: a case study from the Talhar Shale, Pakistan. Arab J Sci Eng, 44(1): 417–428

Ehsan M, Gu H (2020). An integrated approach for the identification of lithofacies and clay mineralogy through Neuro-Fuzzy, cross plot, and statistical analyses, from well log data. J Earth Syst Sci, 129(1): 101–113

Everett J R, Jengo C, Staskowski R (2002). Remote sensing and GIS enable future exploration success. World oil, 223(11): 59–65

Fagin S W (1991). Seismic Modeling of Geologic Structures: Applications to Exploration Problems. Soc Explor Geophys

Fajana A O, Ayuk M A, Enikanselu P A, Oyebamiji A R (2019). Seismic interpretation and petrophysical analysis for hydrocarbon resource evaluation of 'Pennay'field, Niger Delta. J Pet Explor Prod Technol, 9(2): 1025–1040

Fazeelat T, Jalees M, Bianchi T (2010). Source rock potential of Eocene, Paleocene and Jurassic deposits in the subsurface of the Potwar Basin, northern Pakistan. J Pet Geol, 33(1): 87–96

Gee E, Gee D (1989). Overview of the geology and structure of the Salt Range, with observations on related areas of northern Pakistan. Geol Soc America Sps, 232: 95–112

Grelaud S, Sassi W, de Lamotte D F, Jaswal T, Roure F (2002). Kinematics of eastern Salt Range and South Potwar basin (Pakistan): a new scenario. Mar Pet Geol, 19(9): 1127–1139

Guo J, Wei X, Long G, Wang B, Fan H, Xu S (2017). Three-dimensional structural model of the Qaidam basin: Implications for crustal shortening and growth of the northeast Tibet. Open Geosci, 9(1):

174–185

Guo J, Wu L, Zhou W, Li C, Li F (2018). Section-constrained local geological interface dynamic updating method based on the HRBF surface. J Struct Geol, 107: 64–72

Hart B S, Balch R S (2000). Approaches to defining reservoir physical properties from 3-D seismic attributes with limited well control: an example from the Jurassic Smackover Formation, Alabama. Geophysics, 65(2): 368–376

Hesthammer J, Fossen H (1997). Seismic attribute analysis in structural interpretation of the Gullfaks Field, northern North Sea. Petrol Geosci, 3(1): 13–26

Houlding SW (1994). 3D Geoscience Modeling: Computer Techniques for Geological Characterization. New York: Springer Verlag

Ishak M A, Islam M, Shalaby M R, Hasan N (2018). The application of seismic attributes and wheeler transformations for the geomorphological interpretation of stratigraphic surfaces: a case study of the F3 block, Dutch offshore sector, North Sea. Geosciences (Basel), 8(3): 79

Jaboyedoff M, Couture R, Locat P (2009). Structural analysis of Turtle Mountain (Alberta) using digital elevation model: toward a progressive failure. Geomorph, 103(1): 5–16

Jadoon I A K, Hinderer M, Wazir B, Yousaf R, Bahadar S, Hassan M, Abbasi Z H,Jadoon S (2015). Structural styles, hydrocarbon prospects, and potential in the Salt Range and Potwar Plateau, north Pakistan. Arab J Geosci, 8(7): 5111–5125

Jaswal T M, Lillie R J, Lawrence R D (1997). Structure and evolution of the northern Potwar deformed zone, Pakistan. AAPG Bull, 81(2): 308–328

Kadri I B (1995). Petroleum Geology of Pakistan. Islamabad: Pakistan Petroleum Limited

Kazmi A H, Rana R A (1982). Tectonic Map of Pakistan 1: 2000000. Islamabad: Elite Print

Kemal A (1991). Geology and new trends for petroleum exploration in Pakistan. In: Ahmed G, Kemal A, Zaman A S H, Humayon M, eds. New Directions and Strategies for Accelerating Petroleum Exploration and Production in Pakistan. Islamabad: Ministry of Petroleum and Natural Resources: 16–57

Khan M, Ahmed R, Raza H A, Kemal A (1986). Geology of petroleum in Kohat-Potwar depression, Pakistan. AAPG Bull, 70(4): 396–414

Khan M, Liu Y, Farid A, Owais M (2018). Characterizing seismo-stratigraphic and structural framework of late cretaceous-recent succession of offshore Indus Pakistan. Open Geosci, 10(1): 174–191

Khan M Y, Akhter M G, Ahmad Z (2013). Applying gamma-ray logs to a carbonate reservoir: a Pakistan Potwar basin example. Oil Gas J, 111(11): 68–73

Lajaunie C, Courrioux G, Manuel L (1997). Foliation fields and 3D cartography in geology: principles of a method based on potential interpolation. Math Geol, 29(4): 571–584

Mallet J L (2002). Geomodeling. Oxford: Oxford University Press

Mehmood W, Aadil N, Jadoon Y (2016). 3-D Structural modeling of Meyal Field, Potwar Sub-basin, Pakistan using seismic and well data. Nucleus, 53(1): 26–32

Moghal M A, Saqi M I, Hameed A, Bugti M N (2007). Subsurface geometry of Potwar sub-basin in relation to structuration and entrapment. Pakistan J Hydrocarbon Res, 17: 61–72

Muni C, Chaudhry M N, Pervaiz K, Qayyum M, Ahmed R (1990). Geology and structure of Kuza Gali-Dunga Gali-Ayubia area, Hazara-Potwar basin with a reference to hydrocarbon prospects of Attock-Hazara fold and thrust belt. Pakistan J Hydrocarbon Res, 2(2): 43–55

Nanda N C (2016). Seismic Data Interpretation and Evaluation for Hydrocarbon Exploration and Production: A Practitioner'S Guide. New York: Springer

Ngui J Q, Hermana M, Ghosh D, Wan Yusof W I. (2018). Integrated study of lithofacies identification—a case study in X Field, Sabah, Malaysia. Geosciences (Basel), 8(2): 75

Riaz M, Nuno P, Zafar T, Ghazi S (2019). 2D seismic interpretation of the Meyal Area, Northern Potwar deform zone, Potwar Basin, Pakistan. Open Geosci, 11(1): 1–16

Shah S B A, Abdullah W H (2016). Petrophysical properties and hydrocarbon potentiality of Balkassar well 7 in Balkassar oilfield, Potwar Plateau, Pakistan, Bull Geol Soc Malaysia, 62:73–77

Shah S B A, Abdullah W H (2017). Structural interpretation and hydrocarbon potential of Balkassar oil field, eastern Potwar, Pakistan, using seismic 2D data and petrophysical analysis. J Geol Soc India, 90(3): 323–328

Silva C L, Morales N, Crósta A P, Costa S S, Jiménez-Rueda J R (2007). Analysis of tectonic-controlled fluvial morphology and sedimentary processes of the western Amazon Basin: an approach using satellite images and digital elevation model. An Acad Bras Cienc, 79(4): 693–711

Stewart S (1999). Seismic interpretation of circular geological structures. Petrol Geosci, 5(3): 273–285

Szabó N P (2011). Shale volume estimation based on the factor analysis of well-logging data. Acta Geophysica, 59(5): 935–953

Taner M T (2001). Seismic attributes. CSEG Rec, 26(7): 49–56

Wandrey C J, Law B, Shah H A 2004. Patala-Nammal composite total petroleum system, Kohat-Potwar geologic province, Pakistan. Washington DC: US Department of the Interior, US Geological Survey Reston

Wang L, Wu X, Zhang B, Li X, Huang A, Meng F, Dai P (2019). Recognition of significant surface soil geochemical anomalies via weighted 3d shortest-distance field of subsurface orebodies: a case study in the Hongtoushan Copper Mine, NE China. Nat Resour Res, 28(3): 587–607

Wang Z, Gao J, Lei X, Cui X, Wang D (2016). Application of 3D seismic attributes to optimize the placement of horizontal wells within a tight gas sand reservoir, Ordos Basin, China. Geophysics, 81(3): B77–B86

Wellmann J F, De La Varga M, Murdie R E, Gessner K, Jessell M (2018). Uncertainty estimation for a geological model of the Sandstone greenstone belt, Western Australia–insights from integrated geological and geophysical inversion in a Bayesian inference framework. Geol Soc Lond Spec Publ, 453(1): 41–56

Wu Q, Xu H, Zou X (2005). An effective method for 3D geological modeling with multi-source data integration. Comput Geosci, 31(1): 35–43 (J)

Zhang B, Chen Y, Huang A, Lu H, Cheng Q (2018). Geochemical field and its roles on the 3D prediction of concealed ore-bodies. Acta Petrol Sin, 34(2): 352–362